Task Report 2 – Summary of Construction, Trafficking and Monitoring

Project Title: Relative Operational Performance of Geosynthetics Used as Subgrade Stabilization

Submitted By: Eli Cuelho, P.E., Research Engineer
Western Transportation Institute, Montana State University – Bozeman

Dr. Steven Perkins, P.E., Professor in Civil Engineering
Civil Engineering Department, Montana State University – Bozeman

Michelle Akin, P.E., Research Engineer
Western Transportation Institute, Montana State University – Bozeman

Submitted to: Craig Abernathy, Project Manager
Montana Department of Transportation, Research Programs

Date Submitted: February 15, 2013

Introduction

Seventeen test sections were constructed, trafficked and monitored during summer 2012 at the TRANSCEND test facility in Lewistown, Montana to evaluate geosynthetics when used as subgrade stabilization. Design of this experiment was based on previous work completed in 2009 (Cuelho et al., 2009) and centered on providing a uniform platform to evaluate the performance of multiple geosynthetics and other unpaved road design characteristics. This task report documents the basic design attributes of the research test site, material properties and characterization of the various construction materials, how the test site was constructed, an overview of the instrumentation and data acquisition systems, and a description of the trafficking and monitoring efforts.

Design and Layout of Test Site

The design and layout of the test area focused on creating a uniform roadway to study the effects of geosynthetic stabilization, subgrade strength, and base course gravel depth. This required removing the existing roadway and replacing it with a new road that was carefully constructed to minimize or control differences in site characteristics along its length. The TRANSCEND test facility in Lewistown, Montana was used for this research effort.

This research project was specifically planned to quantify differences in performance of various geosynthetic products under the same conditions (i.e., same subgrade strength and base course thickness). In addition, several additional test sections were constructed to study the effect that variations in subgrade strength and base course thickness had on the performance. Specifically, three control sections (i.e., no geosynthetic) were constructed, each having different thickness of

base course aggregate, and three test sections were built using Tensar BX Type 2 geosynthetic, each having different subgrade strengths. The final arrangement of the test sections is shown in Figure 1.

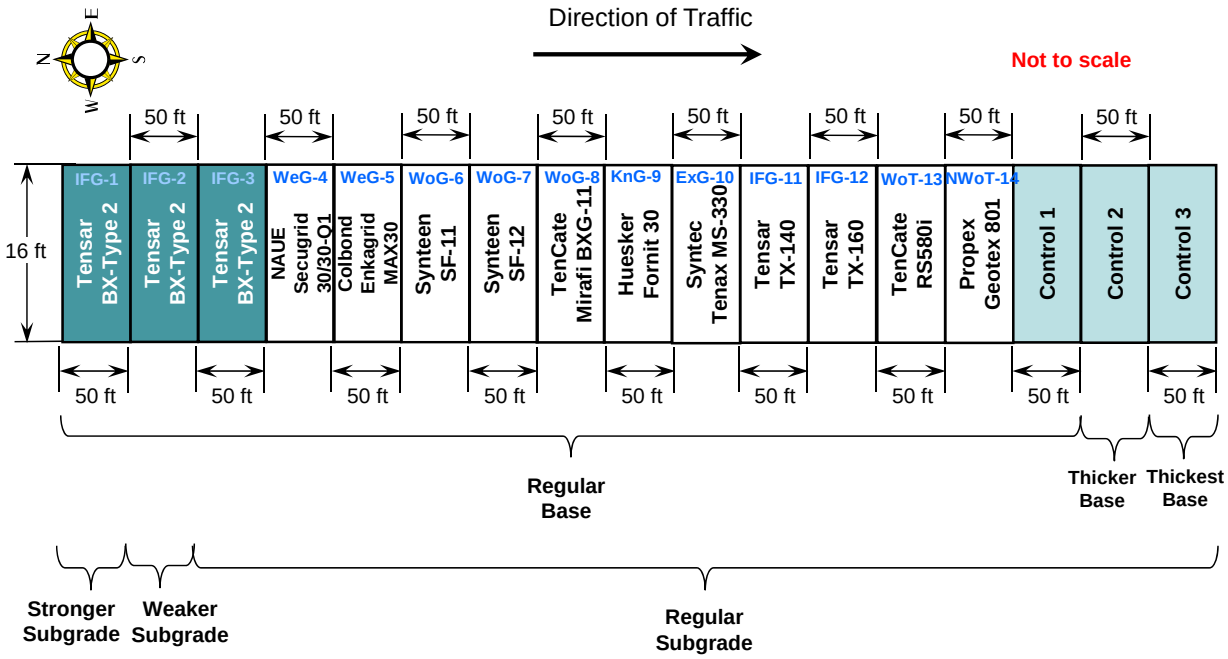

Figure 1: General layout of test sections.

Design of this project is based on a single-lane, gravel road that is built on 3 ft of soft subgrade above a strong, stable substrate. A trench was excavated so the final grade of the test site was similar to the surrounding grade (i.e., the existing taxiway). The size of the excavation was 16 ft wide by 3 ft deep to sufficiently minimize boundary affects from the trench walls and foundation. A length of 860 ft was necessary to evaluate 14 geosynthetic test sections and three control sections. The bottom of the test pit was tapered at the ends to facilitate movement of the construction equipment into and out of the pit. The tapered area was in addition to the 860 ft and was not included in the experiment.

The subgrade was designed to have a slight crown (approximately 1 percent) so that water from precipitation would not pool on the surface. Shaping this crown during construction, however, was difficult to achieve; therefore, the surface of the subgrade followed the slope of the existing taxiway (approximately 1 percent from side to side instead of from the center to the outer edges). The existing surface of the taxiway was originally constructed with approximately 1 percent slope (perpendicular to traffic) to facilitate water egress. The base course (which formed the driving surface) was also to be crowned, but was sloped in the same manner to maintain uniform gravel thickness. The base aggregate extended past the outside edge of the subgrade and tapered down to the existing paved taxiway. Because the final level of the base aggregate was higher than the original level of the taxiway, a gradual ramp was built at each end using the base

aggregate to allow the test vehicle to easily enter and exit the test sections during trafficking. A cross-sectional view of a typical test section is shown in Figure 2 with the test vehicle.

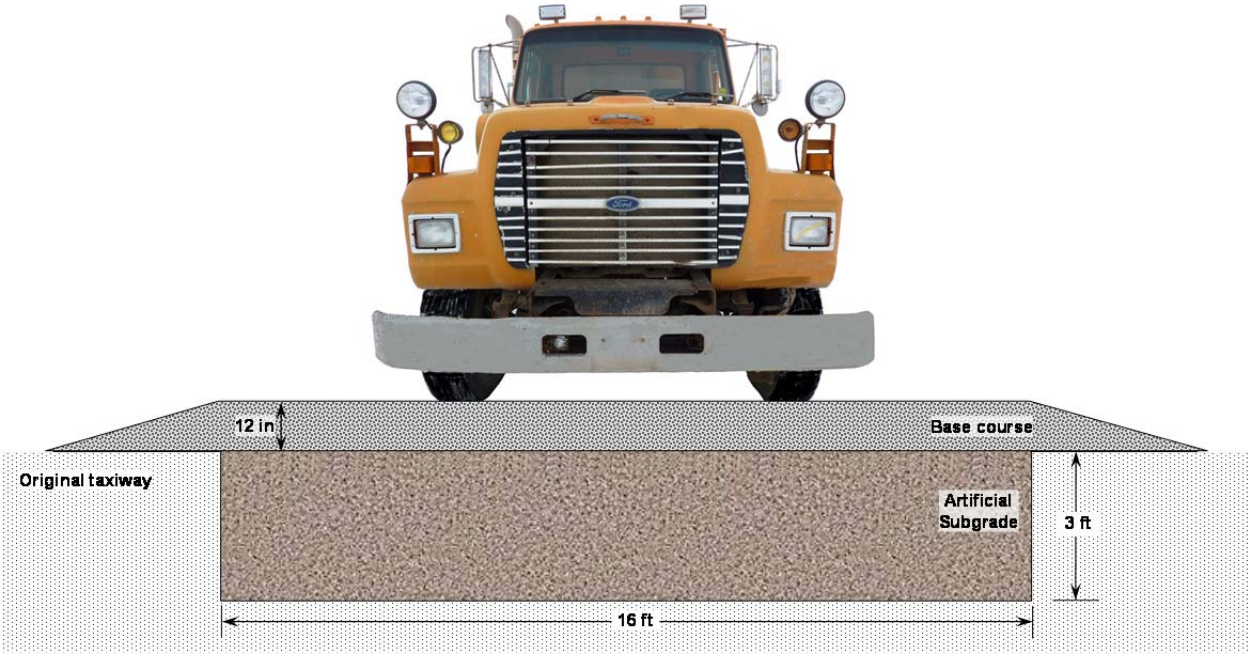

Figure 2. Cross-section of field test section with truck (truck scaled to approximate size).

Artificial Subgrade

The subgrade soil was obtained from a nearby gravel pit, and consisted of natural overburden material that were cleared and stockpiled to provide access to gravel sources below. The material was dried and screened to remove particles greater than 1 inch in diameter, and help blend the stockpile together to ensure uniformity. The subgrade was delivered to the test site and stockpiled adjacent to the trench along the test sections. This soil classified as A-6 according to the AASHTO classification system (AASHTO M-145) or CL (sandy lean clay) according to the USCS classification system (ASTM D 2487). Other relevant properties of the artificial subgrade are listed in Table 1. The gradation for the subgrade material is shown in Figure 3.

Table 1. General Properties of the Artificial Subgrade

Property	
Liquid Limit	34
Plastic Limit	17
Plasticity Index	17
% passing #200 sieve	55%
Max. dry unit weight†	112 lb/ft^3
Optimum moisture content†	16%

† using standard Proctor procedure (ASTM D698)

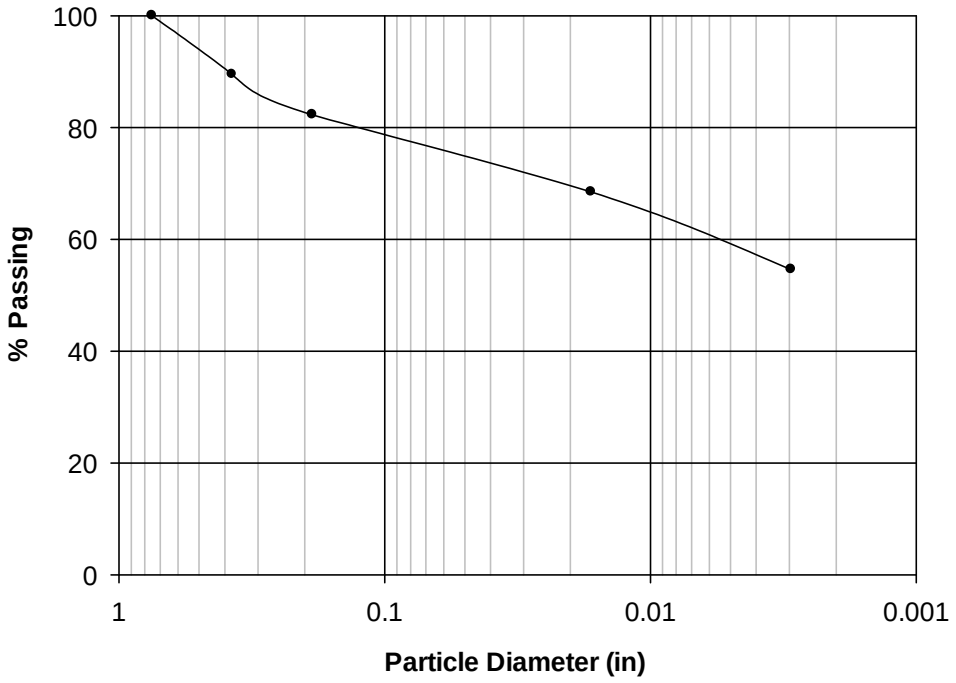

Figure 3. Grain-size distribution of the artificial subgrade soil.

For construction purposes, the subgrade was first characterized in the lab by evaluating the relationship between vane shear strength and California Bearing Ratio (CBR) as the water content was varied. Vane shear tests were conducted on unsaturated, laboratory CBR samples screened to 3/8 in. to relate CBR to vane shear strength. The linear relationship that was developed in the lab using both of these tests resulted in a linear regression R^2 factor of 0.8427, as shown in Figure 4. According to this data, the shear strength as determined using the vane shear device must be between roughly 1,340 and 1,460 lb/ft^2 to achieve a CBR strength of 2.0 ±0.1 (Test Section 1), between roughly 960 and 1,090 lb/ft^2 to achieve a CBR strength of 1.4 ±0.1 (Test Section 2), and between roughly 1,150 and 1,270 lb/ft^2 to achieve a CBR strength of 1.7 ±0.1 (Test Sections 3-C3). Field measurements of shear strength using the hand-held vane-shear device were used as the primary means to characterize the subgrade as it was placed in the open trench because: 1) the device is simple to operate, 2) it provides an immediate assessment of strength, and 3) it was more precise than other devices. A dynamic cone penetrometer (DCP) and lightweight deflectometer were also used as a comparison to monitor subgrade material properties.

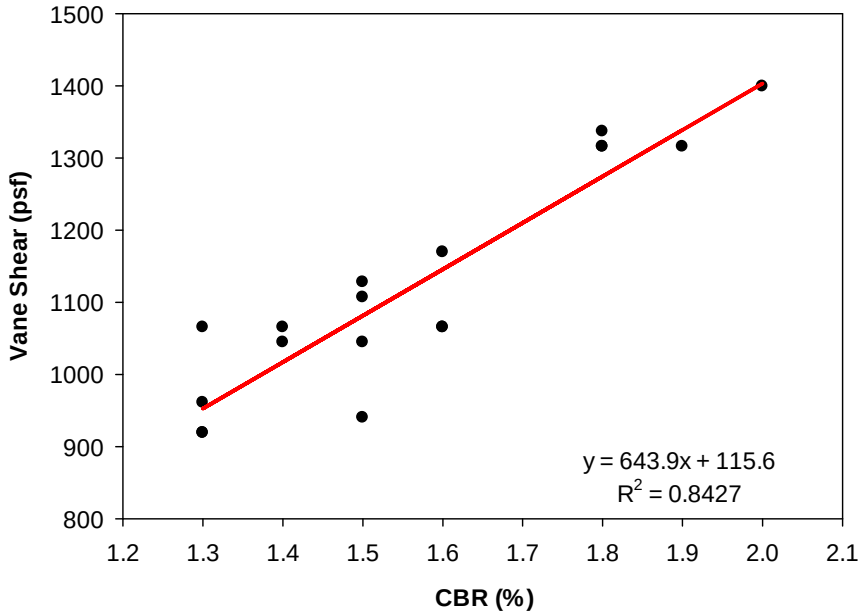

Figure 4: Relationship between California Bearing Ratio and the hand-held vane shear device.

Base Course Aggregate

Base course aggregate specifications were collected from Idaho, Montana, New York, Ohio, Oklahoma, Oregon, South Dakota, Texas and Wyoming (participating states to this pooled-fund research project) to help determine the specifications for the base course aggregate to be used in this research project. Gradation, percent fractured faces, minimum number of fractured faces, sieve size delineating fractured face content, liquid limit and plasticity index were considered as part of this analysis. The percent passing and range of values was averaged for all specifications. In some cases, more than one gradation in a given state was appropriate, so both were included in the analysis. Overall, the combined base course gradation specification is very similar to Montana's 5A Base Course. The Montana 5A specification and the average range of gradations from the various states are summarized in Figure 5 and Table 2.

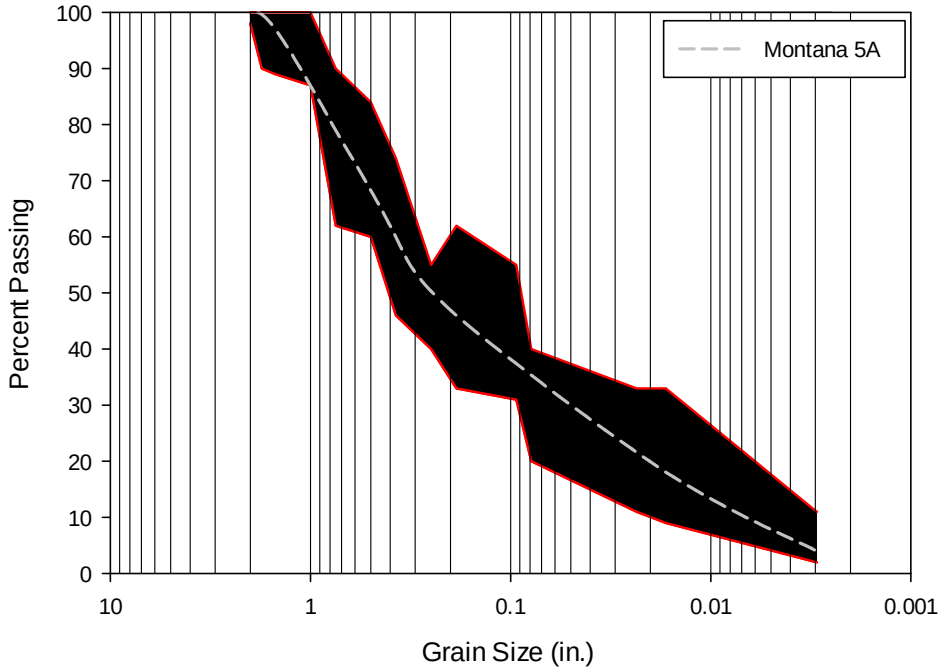

Figure 5: Range of base course aggregate gradations for participating states.

Table 2: Comparison of Montana 5A and Participating States' Average Base Course Gradations

Sieve (US)	Sieve (in)	Montana 5A (% pass.)	Average range (% pass.)
2-inch	2	100	98-100
1 1/2-inch	1.5	94-100	89-100
3/4-inch	0.75	70-88	62-90
3/8-inch	0.375	50-70	46-74
#4	0.187	34-58	33-62
#40	0.0167	6-30	9-33
#200	0.00295	0-8	2-11

In general, fractured faces ranged from no requirement to 100 percent, with the average being between 40 and 50 percent. Most specifications specified a maximum liquid limit of 25 percent and maximum PI of around 6. Considering all of this information, the Montana 5A specification was used as the specification for the base course aggregate for this project with one exception, that the fractured face requirement for material larger than the #4 sieve be increased from 35 percent to 50 percent on at least two faces.

The final base course aggregate for this project was obtained from a gravel pit approximately 20 miles away. The gradation is provided in Figure 6. It classified as A-2-4 according to the AASHTO classification system (AASHTO M-145) or GP-GC (poorly graded gravel with clay with sand) according to the USCS classification system (ASTM D 2487). Other relevant

properties of the base course aggregate are listed in Table 3. CBR tests run on the base course aggregate (ASTM D1883) resulted in bearing ratios that were higher at 0.2 inches displacement than at 0.1 inches displacement, meaning that the CBR at 0.2 inches should be used. Corrections were also necessary to account for the concave upward shape of the load-displacement curve from the CBR tests. These corrections resulted in CBR values greater than 100 for the base course material.

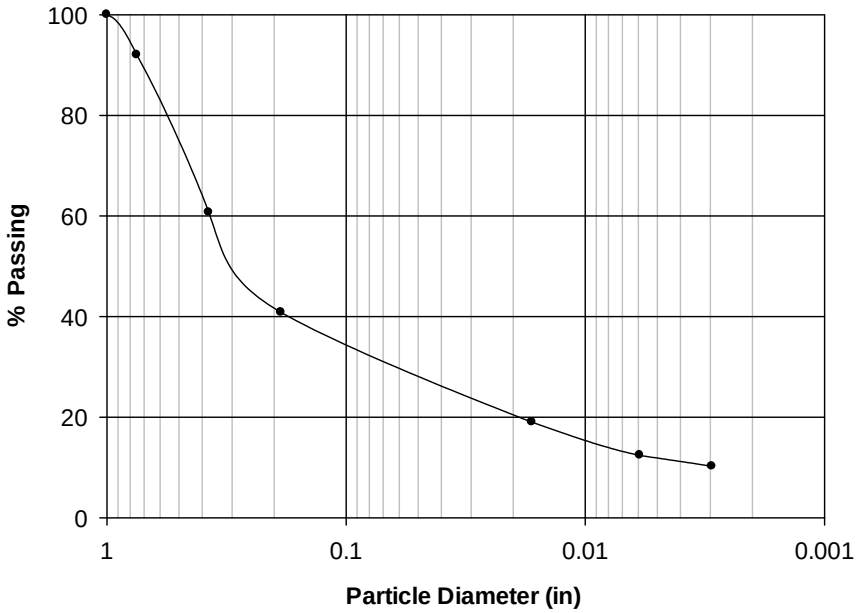

Figure 6. Base course aggregate grain-size distribution.

Table 3. General Properties of the Base Course Aggregate

Property	
Liquid Limit of fines	23
Plastic Limit of fines	15
Plasticity Index of fines	8
% passing #200 sieve	10%
Max. dry unit weight†	139 lb/ft^3
Optimum moisture content†	6.0%
% fractured faces	55%
CBR† (at ρ_{dry} = 140 lb/ft^3)	>100

† using modified Proctor procedure (ASTM D1557)

Separation and filtration criteria were checked using the gradation information from the subgrade and the base course. According to the specifications listed in Holtz et al. (2008), a separation fabric between the base and subgrade is recommended when D_{85} of the base aggregate (D_{85agg} = 0.67 in.) is greater than $5 \cdot D_{85}$ of the subgrade ($5 \cdot D_{85sub} = 5 \cdot 0.3 = 1.5$ in.). In this case, no

separation fabric is required (0.67 in < 1.5 in.). Filter requirements were evaluated by considering the following two criteria: whether the quotient of D_{15} of the aggregate over the D_{85} of the subgrade is less than or equal to 5, and whether the quotient of D_{50} of the aggregate over the D_{50} of the subgrade is less than or equal to 25. For the subgrade and base course materials used in this research project, the first relationship was satisfied, but the second was not.

Reinforced test sections 1 – 14 and control test section C1 were constructed with a target base course thickness of 12 inches. Control test sections C2 and C3 had a target base course thickness of 16 and 24 in., respectively. The base thickness of 12 in. was based primarily on results of box test sections performed at GeoTesting Express (GTX – Alpharetta, GA). Access to results from other test sections constructed at GTX over the past several years was also used.

The test section constructed at GTX for this project used the same subgrade and base aggregate as that used in the full-scale test sections. The GTX test section used 10 in. of aggregate, a peak plate pressure of 90 psi, and Tensar BX Type 2 as the reinforcement. The test section sustained 1,800 load cycles to reach 3 in. of rut depth. The AASHTO equation for equivalent axle load factor was used to compute the equivalent number of ESALs corresponding to the loading conditions used in the GTX facility. A factor of 1.75 was computed, resulting in 3,140 ESALs to reach 3 in. of rut depth.

A load factor of 1.25 was computed using the AASHTO equation for the truck used to traffic the test sections. It was anticipated that no more than 2,000 truck passes would be applied and the expectation was that all sections would reach about 3 in. of rut within 2,000 truck passes. Using a load factor of 1.25, this corresponds to 2,500 ESALs. Comparison of this goal to the results of the GTX test section suggested that the TRANSCEND test sections could be constructed with less than 10 in. of aggregate base. Based on the rapid rutting that occurred in the Phase I project when 8 in. of aggregate was used (Cuelho et al., 2009), by examining other test section results from GTX, and by expecting that truck traffic would be more damaging than cyclic plate loading, the research team did not feel comfortable reducing the aggregate thickness to below 10 in. and felt that a thickness of greater than 10 in. was needed. This was especially true to avoid excessive rutting in the control section. These considerations led to the design thickness of 12 in. of aggregate base. For control sections C2 and C3, aggregate thickness of 16 and 24 in., respectively, were selected to allow base course reduction (BCR) ratios as great as 60 percent to be calculated by comparison of results from reinforced test sections to the three control sections.

Geosynthetics

Twelve geosynthetic products were used in this research project to evaluate their relative performance under the conditions presented herein. A summary of the basic material characteristics of these products is listed in Table 4, and the tensile strength properties, as listed by the manufacturers, are listed in Table 5. Geosynthetic properties were checked against the survivability and apertures size specifications as outlined in Holtz et al. (2008) for stabilization

applications. All of the geosynthetics met the Class 1 survivability requirements (ultimate strength > 1,230 lb/ft for geogrids, and grab strength > 900 lb for geotextiles), but not all geosynthetics met the aperture size criteria. According to the specifications, geogrid apertures must be between 0.5 and 3.0 inches, AND $\geq D_{50}$ of the aggregate above the geogrid, AND $\leq 2 \cdot D_{85}$ of aggregate above the geogrid. The D_{50} and D_{85} of the base aggregate are 0.3 in. and 0.67 in., respectively. All of the geogrids meet the D_{50} requirement, but the apertures of the Colbond – Enkagrid MAX 30 geogrid are large and do not meet this requirement. Even though the aperture size of the SynTec – Tenax MS330 material is large, tripling the material reduces the apparent opening size and helps this material meet this requirement. Likewise the Tensar TX140 and TX160 products, because the apertures are triangular in shape they will also resist material movement between the base and subgrade.

Table 4. Summary of Geosynthetic Characteristics

Geosynthetic Test Section[a]	Product Manufacturer - Name	Structure	Polymer[b]	Roll Width (in)	Mass per unit area (oz/yd^2)	Aperture Size[c] (in) MD x XMD
IFG-1, IFG-2, IFG-3	Tensar - BX Type2	integrally-formed, biaxial geogrid	PP	160	NP	1.0 x 1.3
WeG-4	NAUE - Secugrid 30/30 Q1	vibratory-welded, biaxial geogrid	PP	186	5.9	1.3 x 1.3
WeG-5	Colbond - Enkagrid MAX 30	biaxial, welded geogrid	PP	197	6.0	1.7 x 1.6
WoG-6	Synteen - SF 11	PVC-coated, woven, biaxial geogrid	PMY	186	NP	1.0 x 1.0
WoG-7	Synteen - SF 12	PVC-coated, woven, biaxial geogrid	PMY	183	NP	1.0 x 1.0
WoG-8	TenCate - Mirafi BXG11	PVC-coated, woven, biaxial geogrid	PMY	158	9.1	1.0 x 1.0
KnG-9	Huesker - Fornit 30	polymer-coated, knitted, biaxial geogrid	PP	206	6.5	0.6 x 0.6
ExG-10	SynTec - Tenax MS 330	extruded, triple-layer, biaxial geogrid	PP	156	9.7	1.7 x 2.0[d]
IFG-11	Tensar - TX140	integrally-formed, triaxial geogrid	PP	160	NP	1.6 x 1.6[e]
IFG-12	Tensar - TX160	integrally-formed, triaxial geogrid	PP	160	NP	1.6 x 1.6[e]
WoT-13	TenCate - Mirafi RS580i	woven geotextile	PPF	204	NP	40[f]
NWoT-14	Propex - Geotex 801	non-woven, needle-punched geotextile	PP	186	8.0	80[f]

[a] Acronym meanings (related to manufacturing process): IFG = integrally-formed grid, WeG = welded grid, WoG = woven grid, KnG = knitted grid, ExG = extruded grid, WoT = woven textile, NWoT = non-woven textile; numbers represent position of test section

[b] PP = polypropylene, PMY = polyester multifilament yarn, PPF = polypropylene fiber

[c] MD = machine direction, XMD = cross-machine direction

[d] for a single layer; apparent opening size is reduced when three layers are stacked on top of one another

[e] reported as "rib pitch" in manufacturer's specification sheet

[f] Apparent Opening Size (AOS) in U.S. Standard sieve size, ASTM D 4751

NP = information was not provided by the manufacturer

Table 5. Summary of Geosynthetic Tensile Strength Properties

Geosynthetic Test Section[a]	Strength[b] @ 2% (lb/ft)		Strength[b] @ 5% (lb/ft)		Ultimate[b] Strength (lb/ft)	
	MD	XMD	MD	XMD	MD	XMD
IFG-1, IFG-2, IFG-3	410	620	810	1,340	1,310	1,970
WeG-4	822	822	1,645	1,645	2,056	2,056
WeG-5	754	754	1,576	1,576	2,056	2,056
WoG-6	526	578	792	1,042	2,388	3,870
WoG-7	526	797	1,042	1,367	2,388	5,268
WoG-8	625	625	1,000	1,000	2,500	2,500
KnG-9	410	620	825	1,370	1,700	2,200
ExG-10	418	620	925	1,343	1,370	2,100
IFG-11	NP		NP		NP	
IFG-12	NP		NP		NP	
WoT-13	NP		NP		NP	
NWoT-14	NP		NP		912[e]	

[a] Acronym meanings (related to manufacturing process): IFG = integrally-formed grid, WeG = welded grid, WoG = woven grid, KnG = knitted grid, ExG = extruded grid, WoT = woven textile, NWoT = non-woven textile; numbers represent position of test section
[a] Manufacturers' minimum average roll values (MARV)
[b] ASTM D4595 and ASTM D6637
[c] Tested by WTI as a composite, i.e., not separately
[d] Non-woven portion of this material increases the ultimate strength by 6 kN/m in the MD and by 10 kN/m in the XMD
[e] Grab tensile strength (ASTM D-4632) in Newtons at 50% elongation
NP = information was not provided by the manufacturer

Construction

Construction of the test sections included the following major consecutive steps: excavating and widening the trench, lining the trench with plastic, preparing and placing the artificial subgrade, installing the sensors and geosynthetics, and preparing and placing the base course aggregate. Preparation and construction of the subgrade and base course was monitored extensively to ensure that these materials were placed in a consistent and uniform manner. Each 50-foot long test section was delineated into 14 subsections (seven in each wheel path, labeled *A* through *G*), as shown in Figure 7. A 1.6 ft-long buffer zone at each end of a test section was avoided because the overlap of the geosynthetics coincident with the transitions between adjacent test sections.

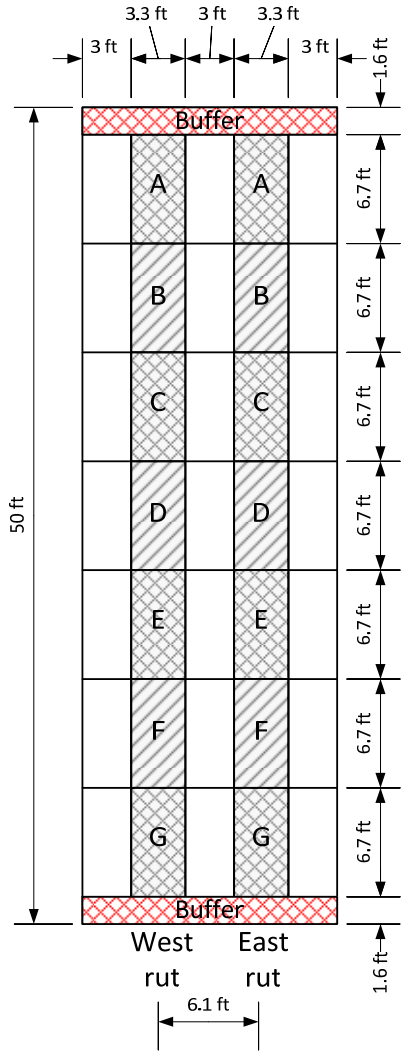

Figure 7: Measurement areas for field soil tests within a single test section.

For quality assurance/quality control during subgrade construction, four measurements of vane shear were made in each subsection for a total of 56 vane shear measurements in each layer in each test section. Six lightweight deflectometer (LWD) measurements were also taken immediately after the layer was compacted. On the final lift of the subgrade, within each test section, 8 dynamic cone penetrometer (DCP) tests, 1 in-field CBR test, and 2 nuclear densometer tests were also conducted. During base course construction, 6 LWD measurements were conducted after the first and final passes of the compactor on the first lift. After the last compactor pass of the final lift, an additional 6 LWD, 6 DCP, 1 in-field CBR, and 2 nuclear densometer tests were conducted. Photos of each of these measurement devices are shown in Figure 8.

Figure 8. Construction quality measuring devices: a) vane shear, b) LWD, c) DCP, d) in-field CBR, and e) nuclear density.

Trench

Construction work for this research project began in late June, 2012 by excavating the materials from an existing trench, and widening and lengthening the trench to its final dimensions of 16 ft wide by 860 ft long. A view of the trench before it was filled with the artificial subgrade is

shown in Figure 9. The floor of the test pit was tapered at the ends to facilitate movement of the construction equipment into and out of the pit; the tapered area was not included in the experiment and is in addition to the 860 feet of length. The trench bottom was compacted with a vibratory roller to provide a stable platform for the remaining construction activities, and was lined with a 6-mil plastic liner to help maintain constructed moisture content of the subgrade throughout the duration of the project (Figure 10).

Figure 9: Completed trench.

Figure 10: Filling lined trench with subgrade.

Subgrade

The subgrade was built in 6 lifts that were approximately 6 inches deep for a total depth of about 3 feet. The subgrade was delivered adjacent to the test pit (refer to Figure 10) and was processed to reach the target strength by adding water from a water truck and fire hose (Figure 11). Water was added until the portion of the pile being prepared reached a target moisture content (e.g., 23 percent for test Sections 3 through C3). Processing was accomplished using a large excavator (Caterpillar 345B). The operator used the bucket to move and mix the material as water was being added (Figure 11). Sufficient material was processed to construct a single 6-inch deep layer over two test sections at a time (about 30 yd^3). The subgrade was then placed in the trench using the excavator and a track-mounted skid-steer tractor was used to level and initially compact the subgrade (Figure 12). A smooth, single-drum, vibratory roller (66-inch wide, 15,500 lb) was used to compact the subgrade by making two passes of the roller in three longitudinal paths of the freshly placed subgrade (Figure 13). The moisture in the top surface of the subgrade was maintained during construction by periodically wetting the surface and keeping it covered with plastic until the next layer of subgrade or the base course could be placed. Prior to placement of the base course, the top surface of the subgrade was smoothed and screeded to the height of the adjacent pavement surface. This was accomplished by tilling the top of the subgrade and pushing a large metal trench box along the surface to remove excess material (Figure 14). The top surface was then re-compacted using a smaller single-drum, vibratory roller. This was done from the side to minimize ruts in the subgrade surface during final

compaction. A topographic survey of the final level of the subgrade was made and the pore pressure sensors were installed prior to placing the geosynthetics.

Figure 11: Watering and mixing subgrade with excavator.

Figure 12: Tracking freshly placed subgrade with track-mounted skid-steer.

Figure 13: Smooth-drum roller used to compact subgrade.

Figure 14: Screeding final subgrade layer.

The upper layers of subgrade are responsible for supporting the majority of the load applied during trafficking. Consequently, the strength of the subgrade at the lower depths was less

important than the strength nearer the surface. In order to characterize the subgrade and assign an average value of strength to each test section, a strategy for weighting the strength of the subgrade layers was developed based on Boussinesq elastic stress distribution theory. Influence values can be determined using Boussinesq's theory based on the area of the load applied at the surface and the depth to the point of interest. Knowing that upper layers have more influence on behavior, the percent of the total influence was determined for each layer and was applied to vane shear measurements in those layers.

The influence value based on Boussinesq's theory (Equation 1) provides the percent of the total influence of each layer, where I_i is the influence value for a particular layer of subgrade. Values for the weighting factor (n_i) for the six subgrade layers were calculated based on the depth of measurement below the finished subgrade surface and actual base course thickness. The approximate weighting factors for individual layers are tabulated in Table 6. The upper three layers of subgrade have the greatest influence (cumulative weight is over 70 percent for these layers).

$$n_i = \frac{I_i}{\sum_{i=1}^{6} I_i} \qquad \textbf{Equation 1}$$

Table 6: Weighting Factors for the Artificial Subgrade

Subgrade layer	Depth to Center of Layer (in)	I_i	n_i
6 (top)	3	0.987	0.317
5	9	0.793	0.255
4	15	0.525	0.169
3	21	0.358	0.115
2	27	0.257	0.083
1	33	0.194	0.062

Composite shear strength was calculated using shear strength from the vane shear device and weighting factors for each layer, according to Equation 2. Composite shear strength values were calculated at regions *A* through *G* within each test section (Figure 15). Most test sections were constructed within ±0.1 CBR of the target. Both the stronger and weaker test sections (target CBR = 2.0 for test section 1 and 1.4 for test section 2) were constructed slightly stronger than targeted.

$$\tau_{composite} = \frac{\sum_{i=1}^{6} n_i \tau_i}{\sum_{i=1}^{6} n_i} \qquad \textbf{Equation 2}$$

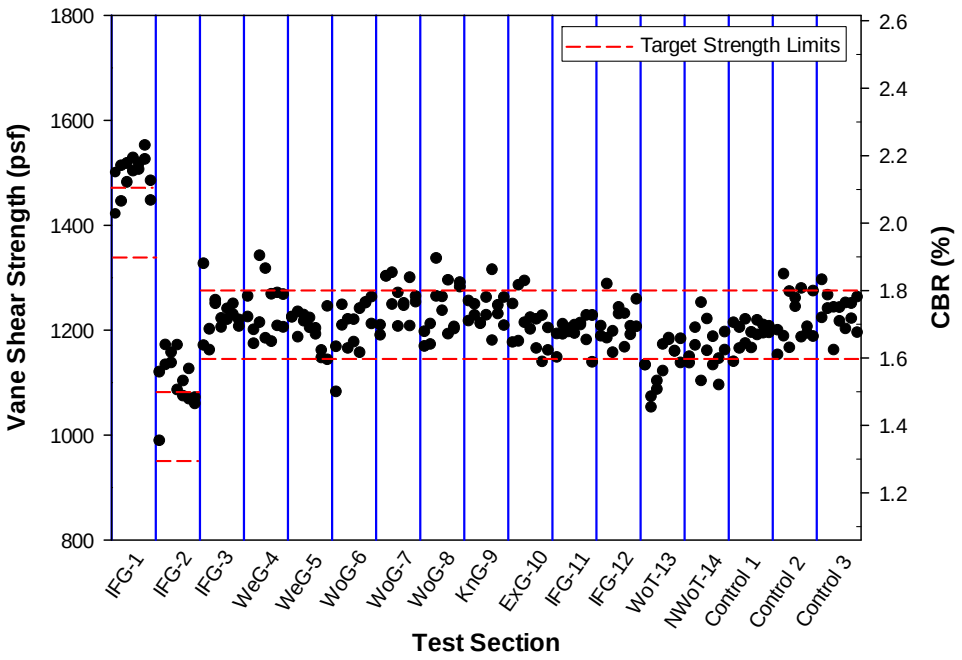

Figure 15: Composite vane shear strength of the constructed subgrade in regions *A–G* (west and east rut paths).

A Zorn ZFG 3000 Light Weight Deflectometer (LWD) was used to measure stiffness within regions *B, D,* and *F* of each layer of each test section during subgrade construction. The LWD has a 1 ft diameter plate, 22 lb drop weight, and provides the dynamic deflection modulus (E_{vd}). The depth of influence for the LWD is about 1 ft, thus measurements on the bottom two layers were neglected due to the presence of the densely compacted fill under the artificial subgrade. Similar to the analysis of vane shear data, a composite E_{vd} was calculated by assigning weights to individual layers using Boussinesq's theory and taking into consideration the measurement depths and base course thickness at individual measurement points. The composite E_{vd} for points within each test section are shown in Figure 16 in comparison to the composite CBR from the vane shear. (A correlation between E_{vd} and CBR was not developed, and the two ordinate axes in Figure 16 are not related.) About half of the test sections show similar behavior regarding E_{vd} and CBR, although there are notable differences for test sections 3–6 where the LWD indicated stiffer subgrade than what was measured by the vane shear.

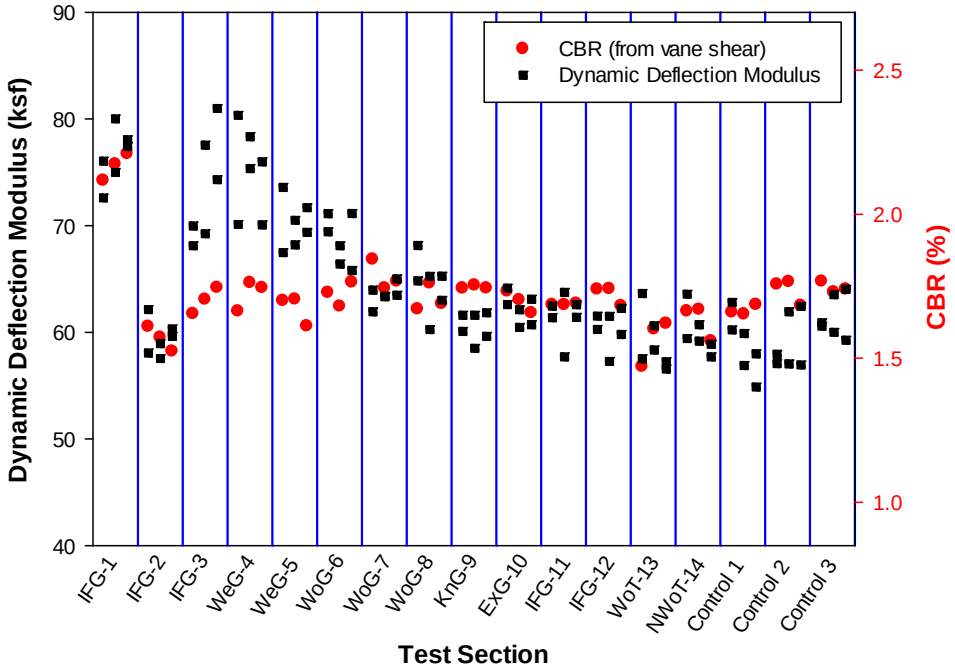

Figure 16: Composite dynamic deflection modulus in regions *B, D,* and *F* (west and east rut paths) of the constructed subgrade and composite CBR from vane shear in regions *B, D,* and *F* (average of west and east rut paths).

A Kessler Dual Mass Dynamic Cone Penetrometer (DCP) with magnetic ruler and a 10.1 lb. hammer was also used to evaluate the strength of the subgrade after it had been fully constructed (i.e., after placement of all six layers), despite the fact that the DCP device was not necessarily well suited to evaluate very small differences in soil strength. The DCP was used in regions *B*, *D*, and *F*, with duplicate measurements in region *D* (for a total of eight measurements in each test section) prior to construction of the base course. Numerous correlation equations exist for converting DCP data to CBR. A number of these relationships were used to compare DCP and vane shear results to identify the most appropriate correlation equation between the two. The original equation (Equation 3, where *DCP* is penetration rate in mm/blow) is one recommended by the US Army Corps of Engineers for CH (fat clay) soils (Kessler, 2010). A modified equation for the artificial subgrade used in this project is shown in Equation 4.

$$CBR = \frac{1}{0.002871\,(DCP)}$$ **Equation 3**

$$CBR = \frac{1}{0.008439\,(DCP)}$$ **Equation 4**

Using this optimized equation and the methodology suggested by Kessler (2010), CBR was calculated as a function of depth. Even with the optimized correlation equation, many of the CBR values were much higher than those estimated from the vane shear data and consistently showed a clear trend of increasing CBR at lower depths due to overburden pressures. Thus a technique commonly applied to Standard Penetration Test (SPT) data for overburden correction was adapted for the DCP analysis. In this case, a correction equation from Peck et al. (1974) was used as the basis for a DCP and CBR depth correction. Data from the vane shear tests conducted on the artificial subgrade were used to modify this equation. The final equation is shown below (Equation 5, where σ_o' is the overburden stress expressed in units of psf). An example of the uncorrected and corrected CBR values (for Test Section 2, region *F*, west rut) is shown in Figure 17.

$$CBR_{corrected} = 1.06\, CBR \log\left[\frac{0.26}{(\sigma_o'/2000\ \text{psf})}\right] \qquad \textbf{Equation 5}$$

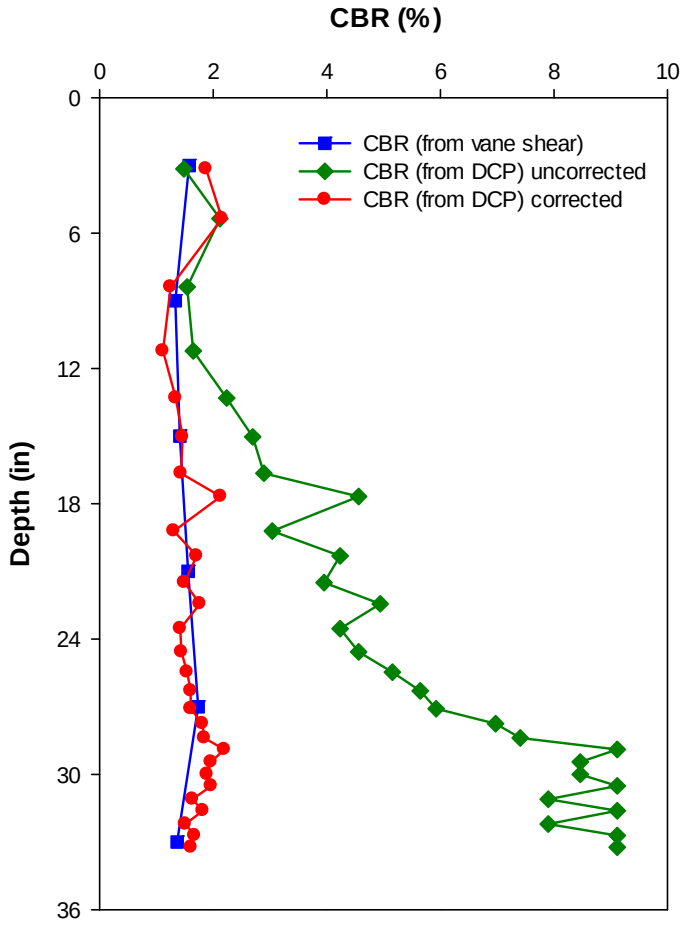

Figure 17: Comparison of corrected and uncorrected CBR results from a typical DCP test on the subgrade (data from Test Section 2, region *F*, west rut path).

As in the previous analysis of the vane shear and LWD data, a weighted average approach was employed to estimate a single composite CBR value for each test section using the DCP data. As before, the influence of the load in the subgrade as a function of depth was calculated using Boussinesq's theory, with adjustments for base course thickness at each measurement point. Weighting factors for the subgrade were calculated as the percent of the total influence at each point using Equation 6, where n_z is the weighting factor at depth z beneath the surface of the subgrade, I_z is the influence factor at depth z, and d_{tot} is the total number of drops to reach depth z. The composite CBR was calculated using Equation 7. Using this methodology, a composite CBR value was calculated for each test section, as shown in Figure 18 along with the composite CBR from the vane shear results. In general, the DCP indicated greater variability in the subgrade than the vane shear.

$$n_z = \frac{I_z}{\sum_{z=1}^{d_{tot}} I_z} \qquad \textbf{Equation 6}$$

$$CBR_{composite} = \frac{\sum_{z=1}^{d_{tot}} n_z CBR_z}{\sum_{z=1}^{d_{tot}} n_z} \qquad \textbf{Equation 7}$$

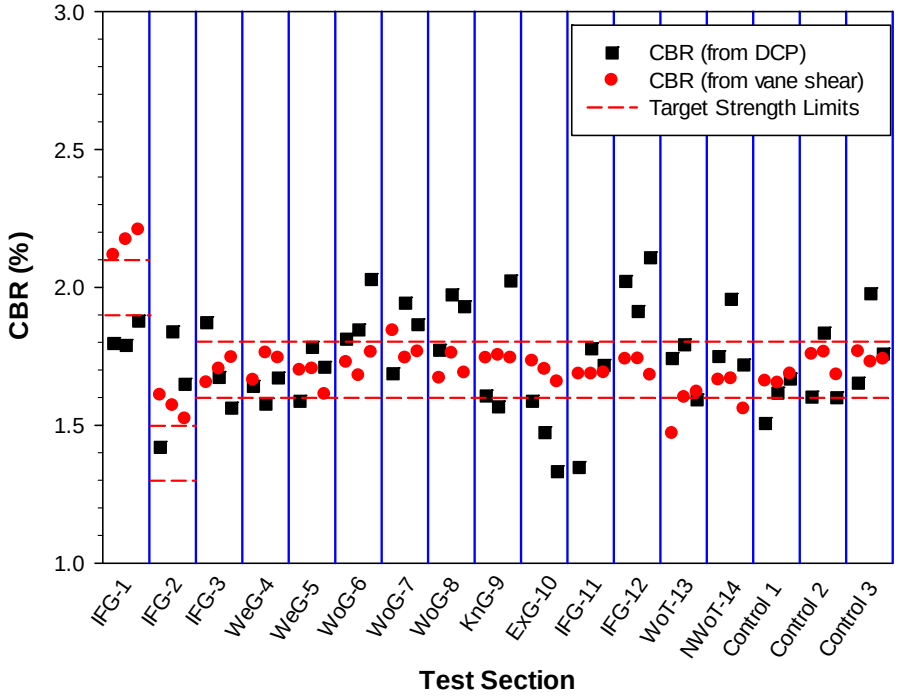

Figure 18: Composite CBR strength of the artificial subgrade from the DCP and vane shear.

In-field CBR tests were conducted on the final layer of the subgrade in substantial accordance to ASTM D4429 with 60 lbs. of surcharge. One test was conducted in each test section, located in region *D* in the west rut. The in-field CBR and the composite CBR determined from vane shear measurements located in region *D* (west rut) are shown in Figure 19. The in-field CBR data is limited and variable, but generally shows that the artificial subgrade is weak (ranging from about 1.3 to about 2.7).

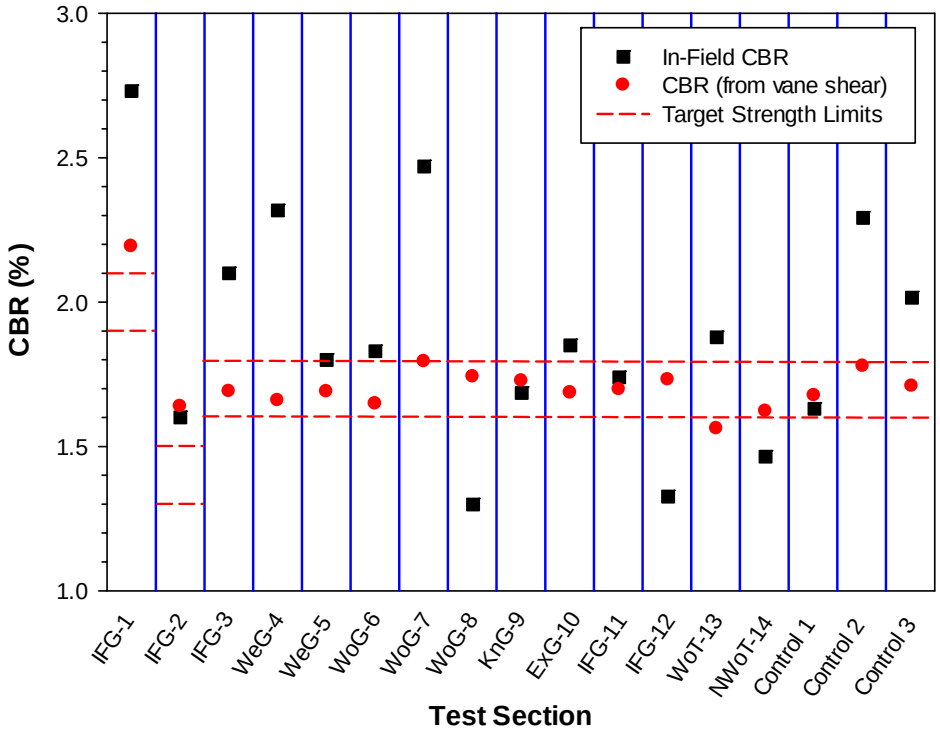

Figure 19: Comparison of subgrade strength from in-field CBR tests and composite CBR from vane shear in region *D* west rut path.

Density of the subgrade was measured with a nuclear densometer in region *D* after the subgrade was constructed. Moisture samples were collected near the density measurements and microwave-dried to determine water content. Test Section 2 had the lowest dry unit weight and the highest water content. Moisture contents at the surface ranged from about 21 to 28 percent, and the dry unit weight ranged from about 100 to 106 pcf (Figure 20).

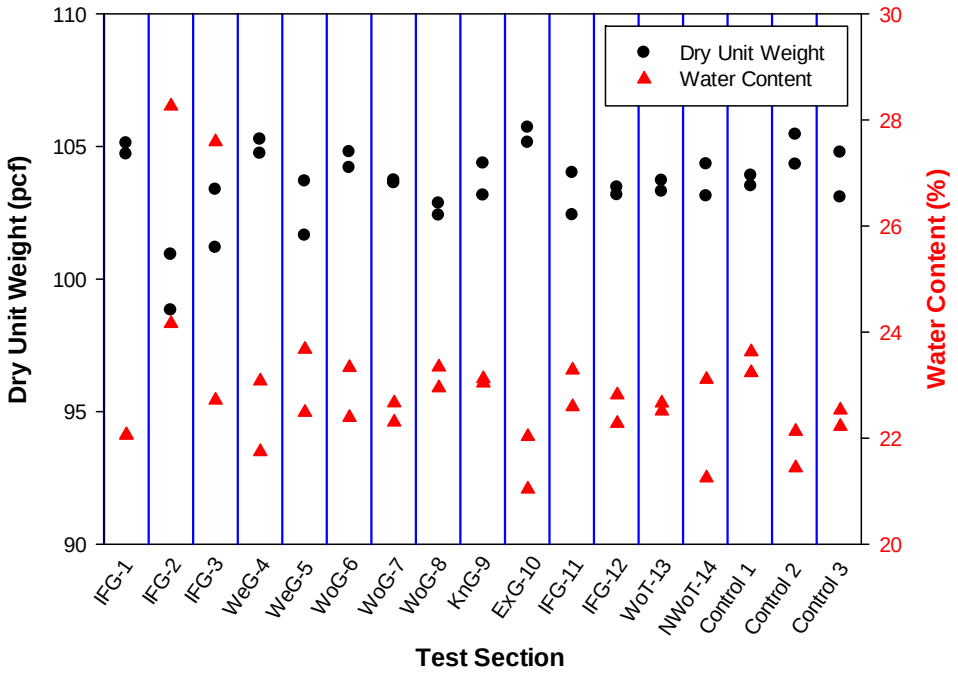

Figure 20: In place density and water content of the subgrade in region *D* (west and east rut paths).

Installation of Geosynthetics

Geosynthetics were delivered to the test site and stored indoors to keep them from exposure to direct sunlight. A single piece of geosynthetic was cut from the roll and strain gages were bonded to the material in two locations prior to installation in the test sections. Geosynthetics were installed on the surface of the subgrade in each test section by carefully rolling them out in the direction of traffic (Figure 21). Any wrinkles were removed by gently pulling on the end of the material. The edges of the geosynthetic were not tensioned or staked in place. Because the widths of the geosynthetics varied between products (as indicated in Table 4), they were centered on the subgrade from side-to-side so that the test vehicle would be centered on the material during trafficking and properly positioned in relation to the displacement, strain and pore-water pressure measurements.

Figure 21: Installed geosynthetic.

Base Course Aggregate

The base course was delivered and stored adjacent to the test sections. Preparation of the base course aggregate began by adding water and mixing with an end loader until it reached optimum water content. A large screed that rested on the paved surface on both sides of the subgrade trench was used to level the surface of the gravel layer (Figure 22). The base course was placed in two layers. The final thickness of the first layer of base course was about 8 inches when compacted and the second was about 3 inches deep for a total of about 11 inches of gravel, on average. The two control test sections contained thicker base material. The Control 2 test section was constructed of two layers of about 8 inches thick, for a total of about 16 inches of gravel when compacted, and the Control 3 test section was constructed of three layers of about 8 inches thick, and had a final average thickness of 25 inches of gravel when compacted. The final thickness of the base course in each test section is shown in Figure 23. Compaction was achieved using a smooth, single-drum, vibratory roller (54-inch wide, 12,000 lb). In total, eight passes of the roller were made per lift at three transverse positions. In addition to a topographic survey, the final gravel surface was measured using DCP, LWD, CBR, and nuclear densometer.

Figure 22: Screeding gravel surface.

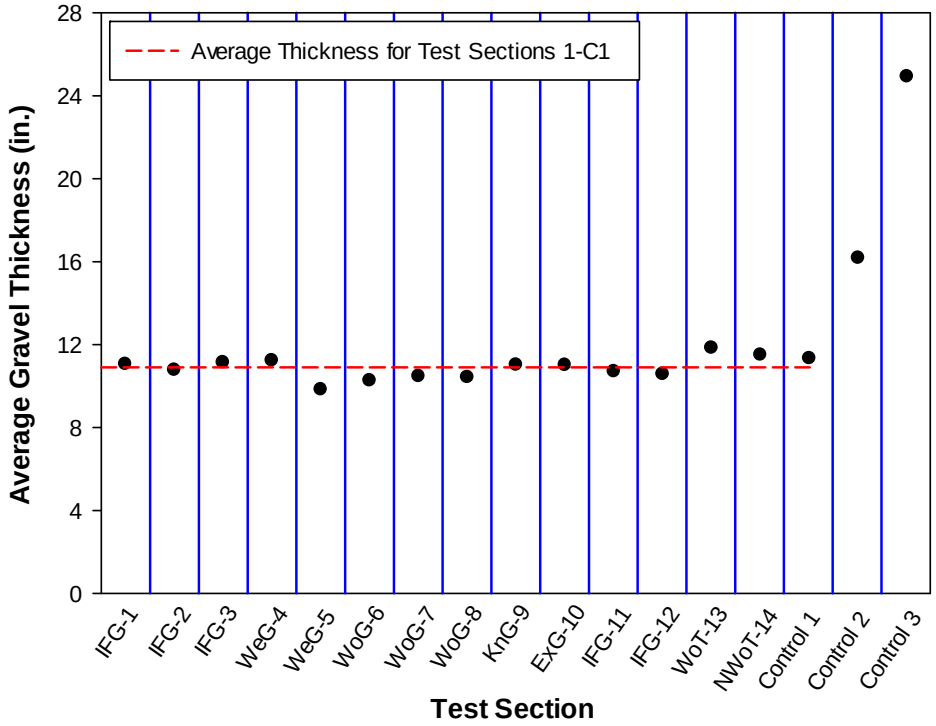

Figure 23: Average base course thickness.

DCP measurements were taken with the dual mass DCP (drop hammer weight of 17.6 lbs.) on the finished surface of the base course in regions *B, D,* and *F* in the west and east rut paths. A correlation equation recommended by the US Army Corps of Engineers for granular soils was used to convert the DCP data to CBR strength (Equation 8, where *DCP* is penetration rate in mm/blow). Penetration data from the upper and lower 2 in. of the base were not used in the calculation of average CBR for each region—granular materials near the surface of the gravel were more easily disturbed, being unbound and the lower 2 in. was close enough to the weak subgrade soil to influence DCP measurements. The variation of CBR along the test plot (as determined from the DCP measurements) is shown in Figure 24. Test sections 1–8 generally showed lower CBR strength than other test sections. The average CBR of the base course was about 20.

$$CBR = \frac{292}{(DCP)^{1.12}} \qquad \textbf{Equation 8}$$

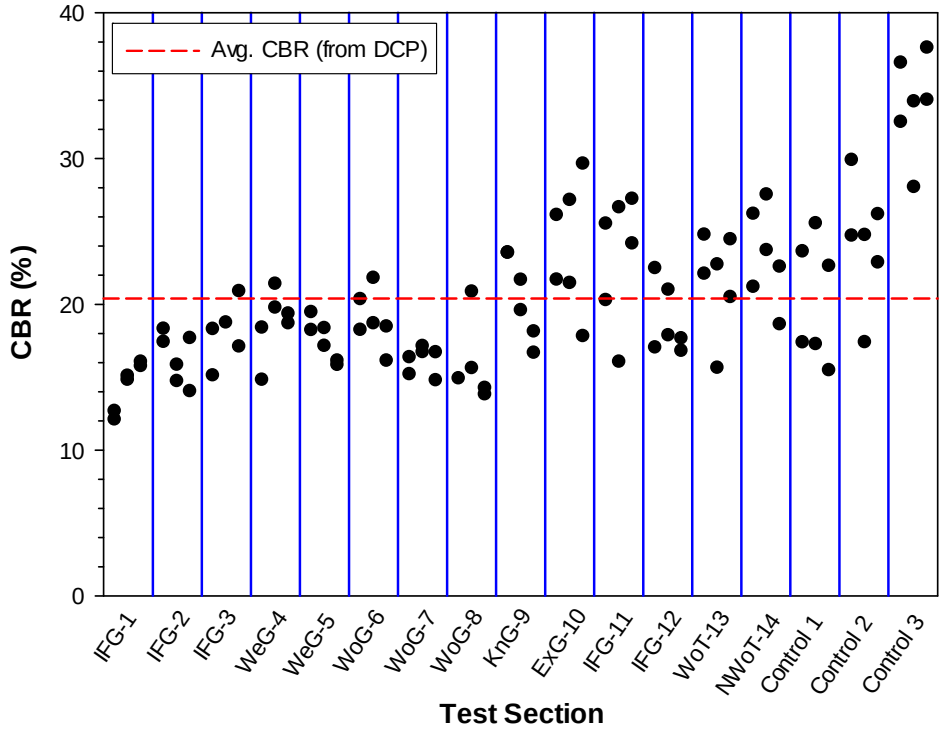

Figure 24: Base course CBR strength from DCP measurements in regions *B, D,* and *F* (west and east rut paths).

LWD measurements were conducted during and after construction of the base course in regions *B, D,* and *F* in the west and east rut path (total of 6 measurements in each test section). The first LWD measurements were made after the first lift of gravel was placed and compacted with one complete pass of the vibratory roller (made up of two individual passes, one up and one back). Three additional complete roller passes were then made (six individual up and back passes)

before the second set of LWD measurements were made on the first lift. Final LWD measurements were made after the second lift was placed and compacted with four complete (eight individual) roller passes. Only Control 3 required a third lift and third set of LWD measurements, again, with four complete (eight individual) roller passes.

The average dynamic deflection modulus from the LWD for each test section is shown in Figure 25 (average of the six results from regions *B, D,* and *F*, west and east rut paths). The base course modulus along the test site was fairly consistent after the first lift with an average value of 188 ksf and standard deviation of 25 ksf. The difference in modulus between the first and final roller pass was inconsistent along the test site. Some test sections exhibited stiffer moduli after additional compaction, whereas others showed similar or weaker moduli. The average difference across the test site was only a 3 ksf increase, however the maximum increase was 64 ksf and the maximum decrease in modulus was 47 ksf. Three of the eight test sections that showed an increase in modulus were the unreinforced control sections. The subgrade likely has some effect on the LWD measurements on base course, particularly with the first lift.

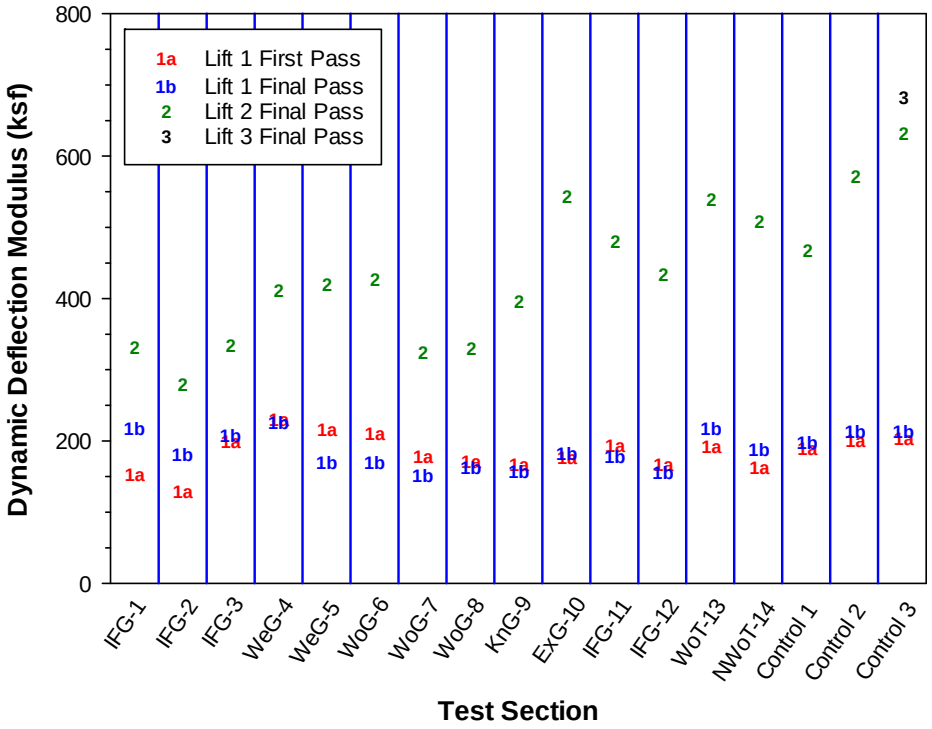

Figure 25: Average LWD measurements during and after base course construction.

The dynamic deflection modulus from the final set of LWD measurements after the base course was fully constructed exhibits similar behavior in comparison to the average CBR of the base course as determined from DCP measurements (Figure 26). The southern test sections are consistently stiffer than the northern test sections.

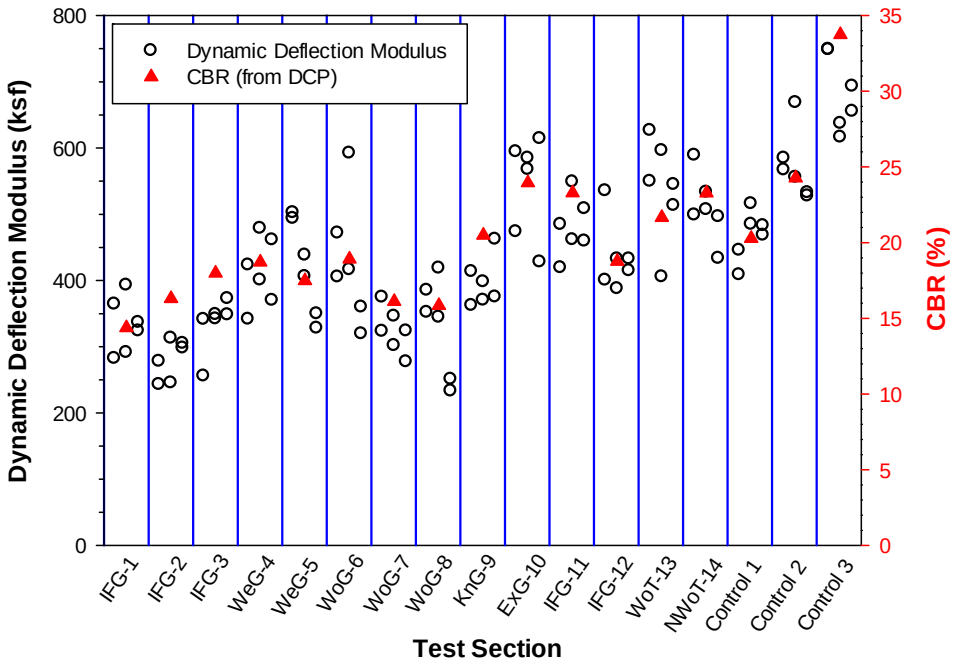

Figure 26: LWD (regions *B, D,* and *F,* west and east rut paths) and average CBR from DCP measurements of the completed base course.

In-field CBR tests were conducted after construction of the base course, in substantial accordance to ASTM D4429 using 30 lb of surcharge. One test was conducted in each test section, located in region *D* in the east rut. The in-field CBR for each test section is shown in Figure 27. The in-field CBR test results demonstrate a similar trend to the LWD and DCP measurements in that the southern test sections are generally stronger and stiffer than the northern test sections. The in-field CBR results were about 2.6 times greater than the CBR calculated from DCP data. Since only one test was conducted on the final subgrade surface in each test section, the in-field CBR data is not considered as reliable an indicator of overall strength or variability.

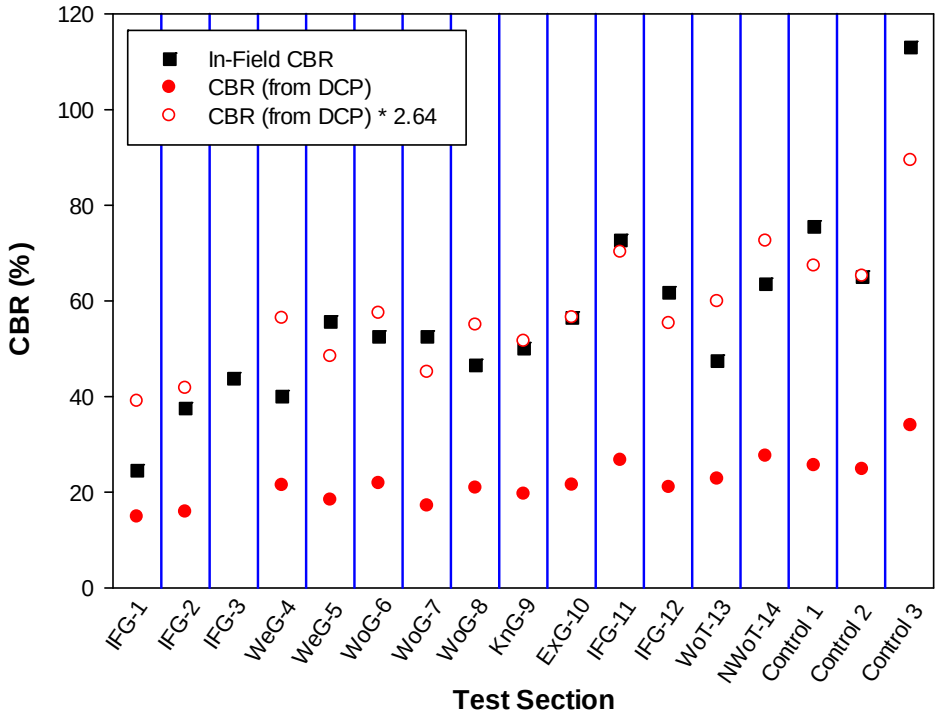

Figure 27: Comparison of base course strength from in-field CBR tests and CBR from DCP in region *D* (east rut path).

A nuclear densometer was used to measure density and water content during and after construction of the base course in region *D* in both the east and west rut paths. The average dry unit weight and water content in region *D* of the constructed base course of each test section is shown in Figure 28. All test sections achieved the minimum compaction specification of 95 percent of maximum dry density (determined according to ASTM D1557, modified Proctor).

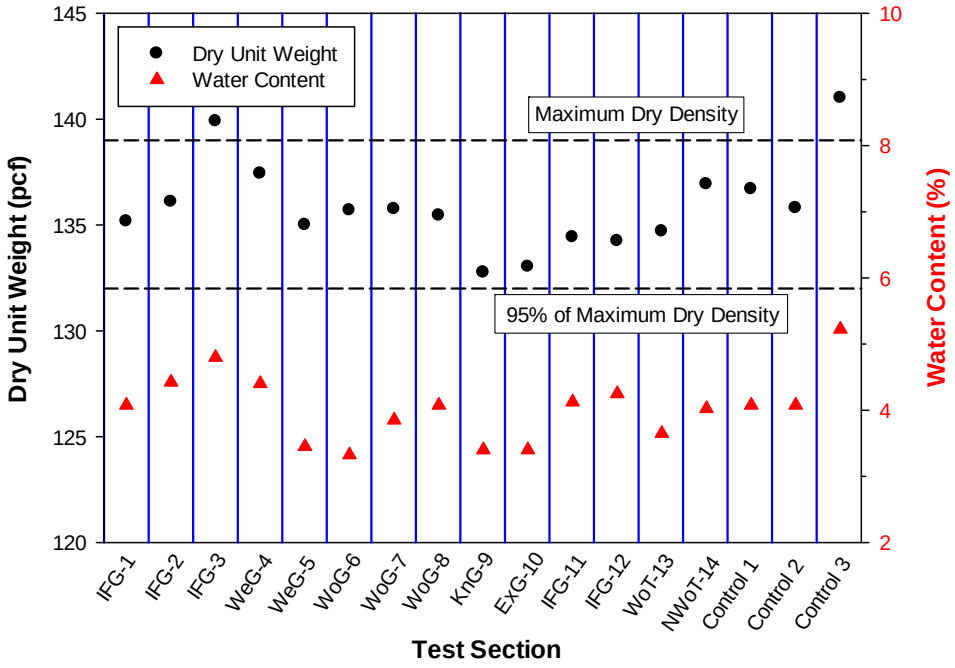

Figure 28: In place density and water content of the base course.

Instrumentation and Data Acquisition Systems

Instrumentation was used in this research project to measure displacement and strain on the geosynthetic (in the cross-machine direction) and pore-water pressure in the subgrade. Linearly variable displacement transducers (LVDTs) were used to measure displacement, resistance strain gages bonded to the surface of the geosynthetics were used to measure strain, and pore-water pressure gages were used to measure pore pressures in the subgrade. Data from the sensors were collected and stored using two CR9000 data loggers from Campbell Scientific, Inc., which were housed in a mobile laboratory located adjacent to the test site.

Six measurements of transverse displacement of the geosynthetic and three measurement of pore pressure in the subgrade were measured at a two separate locations within each test section, as illustrated in Figure 29. A cross-sectional of the layout of the sensors at each location is illustrated in Figure 30. All sensors and associated electronics were mounted in watertight enclosures that were rigidly attached to the existing pavement away from the edge of the test pit to minimize the influence of the presence of these gages in the rut bowl area (Figure 31). The two enclosures were centered in each test section and separated 15 ft from one another. Flexible conduit was used to protect instrumentation cabling. One of the boxes was designated as the "master", which was directly wired to the data acquisition computers that were housed in the mobile laboratory. The other enclosure ("slave") was wired through its corresponding master.

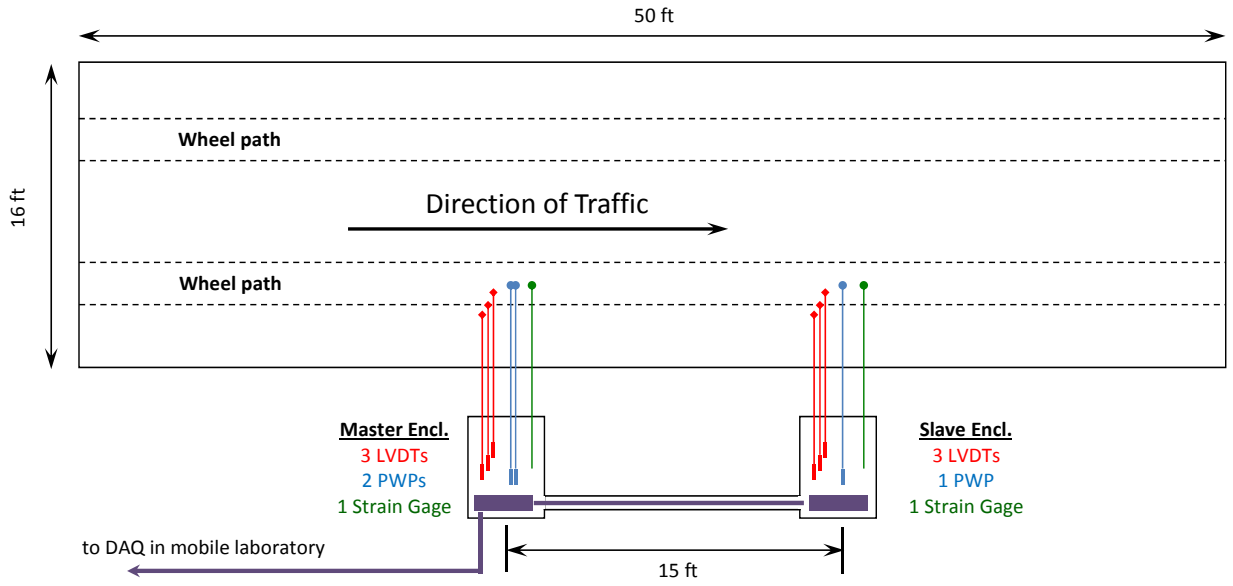

Figure 29: Illustration of instrumentation arrangement within a single test section.

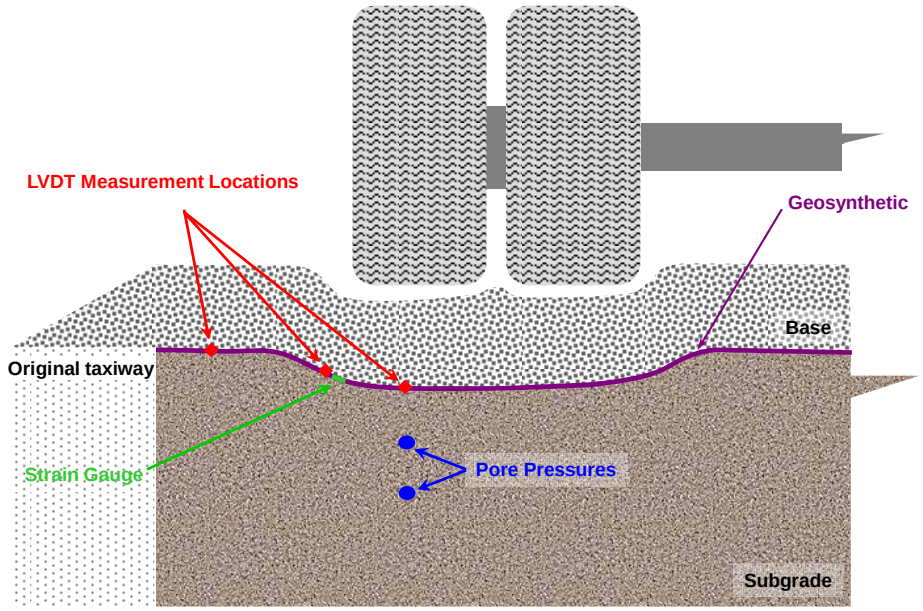

Figure 30. Cross-sectional view of instrumentation layout.

Figure 31. Instrumentation enclosure mounted to pavement.

Displacement Measurements

Six displacement measurements per test section were made – three measurements at two separate locations. These sensors were rigidly attached to the bottoms of the enclosures so that the displacement measurements could be made relative to a fixed reference point outside of the test sections. Lead wires were attached to the geosynthetic to bring the point of measurement on the geosynthetic back to the sensor. Rigid plastic tubing was run inside small diameter, schedule 80, PVC pipes to further protect the plastic tubing during trafficking and to plumb the lead wires into the sensor box. A completed lead wire installation and protective tubing arrangement is provided in Figure 32.

Figure 32: Typical lead wire installation with protective tubing.

Resistance Strain Gages

Resistance strain gages were used to measure the strain response on the transverse reinforcing members of the geosynthetic. Gage selection was done mainly based on their size in relation to the size of the elements they need to be mounted on. The EP series of strain gage (from Micro-Measurements – Raleigh, NC) was selected because it accommodates large strain measurements (± 20 percent in some cases).

Instrumenting strain gages on geogrids consists of six main steps: 1) preparing the strain gages, 2) preparing the geogrid surface, 3) attaching the strain gages to the geosynthetic, 4) curing the adhesive, 5) attaching the instrumentation wiring, and 6) applying and curing the protective coating. Strain gaging took place in an enclosed building at the TRANSCEND research facility in Lewistown to minimize influences from wind, sun, water, and airborne contaminants.

Preparation of the strain gages consisted of attaching wires from the strain gage to bondable terminals. The reason for this step is to prevent potential forces transmitted along the instrumentation wire from damaging the strain gage or affecting its performance during installation and trafficking. Two examples of a typical setup of the gage with jumper wires attached are shown in Figure 33. Special solvents were used to clean the strain gages after this step to remove any foreign matter or solder residues prior to bonding.

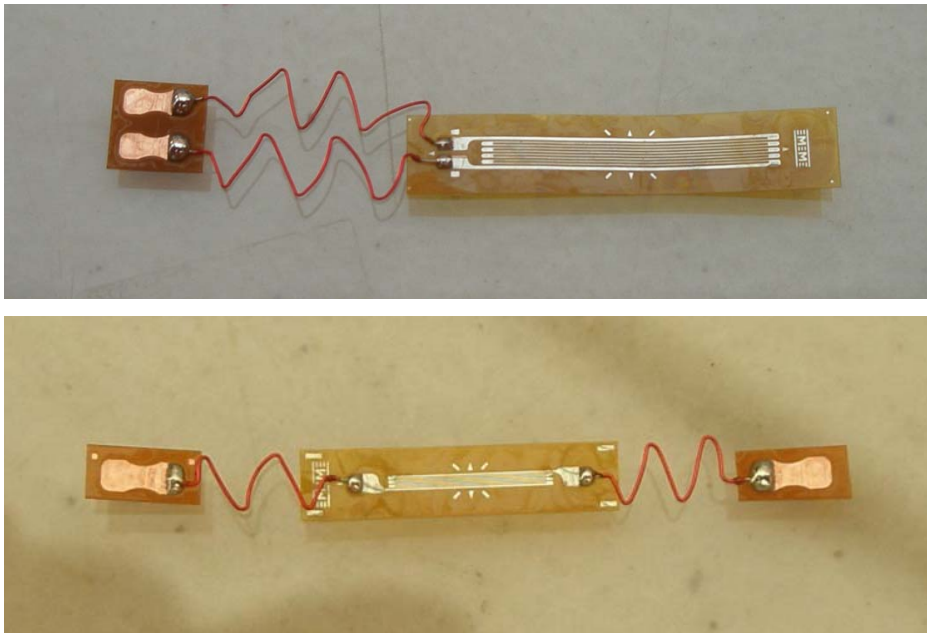

Figure 33: Jumper wires attached to strain gages.

The surface of the geogrid was thoroughly cleaned before applying the adhesive and attaching the strain gage. Preparation of the surface consists of degreasing the surface using a solvent, lightly abrading the surface with sandpaper, and applying chemical conditioning and neutralizing agents. For the woven geogrid products, the protective PVC or polymer coating, applied by the manufacturers to protect the woven grid structure, was removed prior to the cleaning and prepping process. The solvent degreaser removes oils, greases, organic contaminants, and soluble chemical residues. Abrading the surface removes any surface defects of the geogrid, and lightly roughens the surface to facilitate bonding of the adhesive. The conditioning and neutralizing solutions bring the surface to an optimum pH of 7.0 to 7.5.

The strain gages are positioned on the material, the adhesive is applied and, pressure is applied to the gages to create an optimum bond. Two gages were attached to the material at a single location (one on the top of the geosynthetic and one on the bottom) to negate the effects of local bending of the gaged area. Strain gages were attached to the transverse ribs of the geogrids, or in the transverse direction of the geotextile to measure strain in the transverse direction during trafficking. Curing of the adhesive was achieved by elevating the temperature to 150 °F for 6 hours in the gage area. Excess glue was carefully removed using a dremel tool and the lead wires were attached. A strain gage bonded to a geogrid is shown in Figure 34.

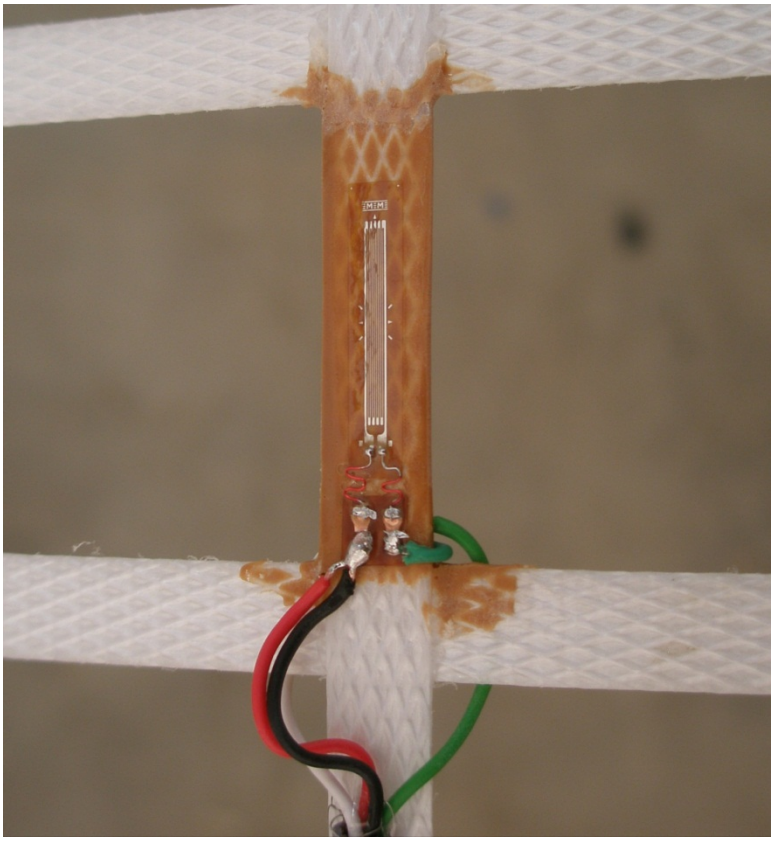

Figure 34: Completed placement and wiring of a strain gage.

A protective coating is then applied to keep water from entering the gaged area and to protect it from physical damage during construction and trafficking. M-Coat J from MicroMeasurments Group was used for this purpose. A thin piece of Teflon™ is used to separate the exposed gage surface from the coating material, as recommended by the manufacturers. Curing of the protective coating was accelerated by heating the gage area to 125 °F for 2.5 hours. A finished strain gage location is shown in Figure 35.

Figure 35: Completed strain gage installation with protective coating.

The procedure used to bond strain gage to geotextiles was similar, but modified slightly to accommodate the unique surface structure of the materials. To minimize stiffening of the gaged area, a different adhesive (a non-conducting silicone) was used to bond the strain gages to the textiles and also act as the protective coating. A completed strain gage installation on the geotextiles is shown in Figure 36.

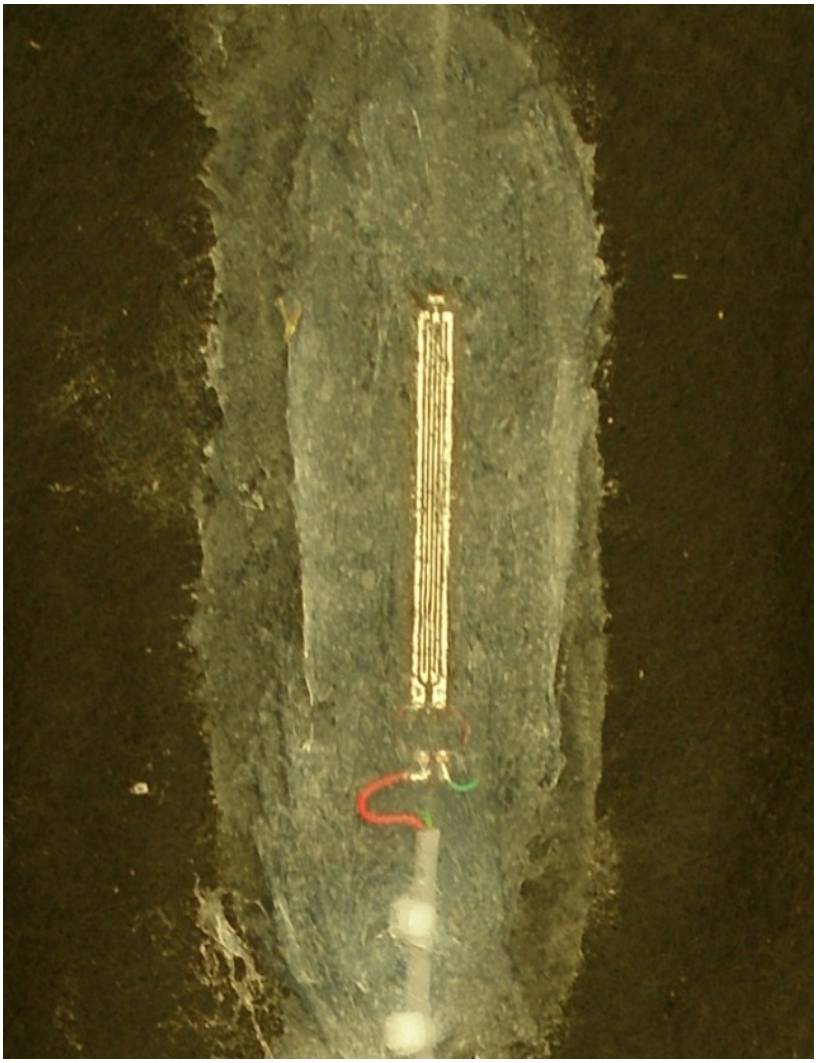

Figure 36: Completed strain gage installation on a non-woven geotextiles.

A three-wire lead wire system was used to negate influence from long lead wires between the strain gage area and the Wheatstone bridge circuitry. Shunt calibration of the strain gage was done to ensure proper operation and determine the baseline measurement for the gages prior to installation.

Pore-water Pressure Gages

Pore-water pressure measurements in the subgrade were made using a pressure transducer (0 to 30 psi range) connected to a porous ceramic stone via a rigid plastic tube. The rigid tubing and porous stone extended the point of measurement from the rut area to the pressure sensor which was housed in the enclosures adjacent to the test sections. An extensive laboratory evaluation was undertaken to verify the performance and accuracy of the pressure sensors prior to installing them in the field. This verification process included testing the sensor at various pressures while in a water bath and while embedded in the subgrade soil. In-water tests were used to verify the sensor and associated electronics were working as expected. In-soil tests were conducted by

preparing the subgrade to the target strength (CBR = 1.7), and subjecting them to anticipated stresses that were generated during construction and trafficking. Results from these tests indicated that the sensors, when properly prepared, should yield meaningful and accurate responses for analysis purposes.

Based on the laboratory work, a protocol was developed for attaching the porous ceramic stones to the high strength, flexible tubing and de-airing the tubing, sensor and porous stone assembly. The porous ceramic stones are specially made for soil pore-water pressure measurement applications (k = 7.56 x 10^{-7} cm/s, porosity ≈ 34%, effective pore size = 1.7 microns). These stones were attached to the flexible tubing using a special epoxy to prevent leakage of water and entrance of air during their installation and use. The water used to fill the sensor, tubing and saturate the stone was de-aired by boiling and vacuum methods. The ceramic porous stones were also saturated by boiling them (Figure 37). Vacuum pumps were used to pull the de-aired water through the saturated stone and into the flexible tubing. A brass fitting was used to attach the open end of the flexible tubing to the sensor. This was done under water to prevent any air from penetrating into the system during assembly. This procedure was used to prepare all of the pore-water pressure sensors used in this research project. Great care was given to the de-airing and preparation process to ensure that no bubbles were present in the flexible tubes during installation and use.

Figure 37: Saturation of ceramic porous stones.

Three pore-water pressure measurements were made in each test section, including the controls. Two measurements were made at 6 in. depth and a single measurement was made at 10 in. depth

in the wheel path. A small hole was excavated in the subgrade and the saturated stone was covered with a layer of very wet subgrade just prior to being placed at the appropriate depth (Figure 38). This wet soil was needed to prevent the soil from drying out over time. The remainder of the hole was then filled with subgrade and the flexible tubing was run through protective conduit. Using these installation techniques, all pore water pressure sensors were active and in good working condition after construction. During the trafficking phase, however, air bubbles were noticed in several of the sensors. The pore-water pressure sensors were removed in late October to prevent damage to the sensors from below-freezing temperatures.

Figure 38: Installation of pore water pressure sensor in subgrade.

Data Acquisition and Power Systems

The data acquisition system consisted of two CR9000 data loggers from Campbell Scientific Inc. (Logan, UT) that were housed in a mobile laboratory centrally parked near the test site. Data cabling from each of the test sections were routed through flexible conduit and buried adjacent to the test sections to transmit data from and power to the sensors housed in the enclosures. Cabling was connected to circuitry located in the mobile lab to facilitate measurements from each of the sensors (Figure 39). Solar power was planned for this project, but current demand from the sensors and data loggers was too high. After several attempts to make this system work, AC power was eventually installed.

Long term data were recorded from all of the sensors every 30 minutes during the trafficking phase. The data loggers were also used to record dynamic data (at 25 Hz) from all of the sensors

during passage of the truck. These dynamic data were recorded during truck passes 1, 2, 3, 5–10, 20, 40, 140, 175, 251, 301–303, 391–395, and 546–548.

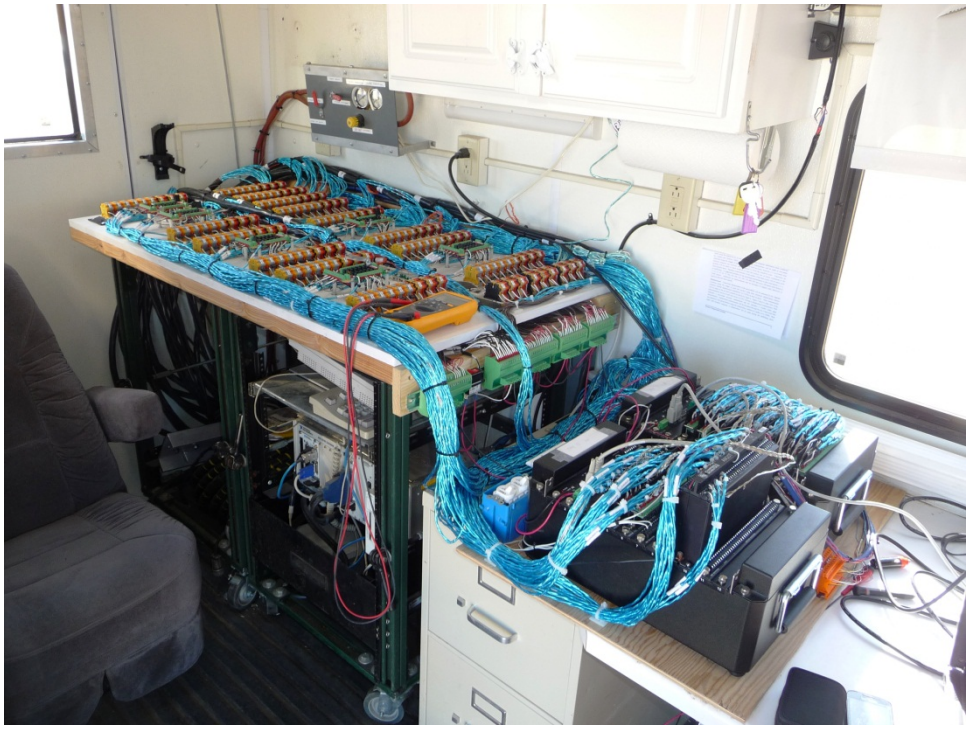

Figure 39: Completion circuitry and data loggers in mobile laboratory.

Trafficking and Data Collection

Trafficking began on September 13th and continued until November 7th, using a three-axle dump truck that weighed 45,420 lb (Figure 40). Dimensions and weights of the individual axles are shown in Figure 41. Trafficking was always in one direction, and the speed was approximately 5 mph to ensure that dynamic loads were not induced in the test sections from any unevenness in the gravel surface. Longitudinal lines were painted on the gravel surface to position the truck during trafficking. These painted lines were also used to mark where rut measurements were to be made. Occasional rainstorms having accumulations greater than one-tenth of an inch over a 24 hour period interrupted trafficking. A total of 1.4 in. of rain fell during the course of trafficking the test sections. A history of the precipitation during trafficking is presented in Figure 42. Traffic resumed once the surface of the gravel had dried significantly. Trafficking continued until rut levels reached 3 inches – defined as failure in this project. Once 3 inches of rut was attained, repairs were made by placing additional gravel in the rutted areas using a skid-steer loader and leveling the surface (Figure 43). Repairs within test sections were made incrementally, so that un-failed portions of test sections could continue to be trafficked until they reach failure. No further measures of rut were made in areas that were repaired. A history of the rut repair is provided in Appendix A.

Figure 40: Three-axle dump truck used for trafficking.

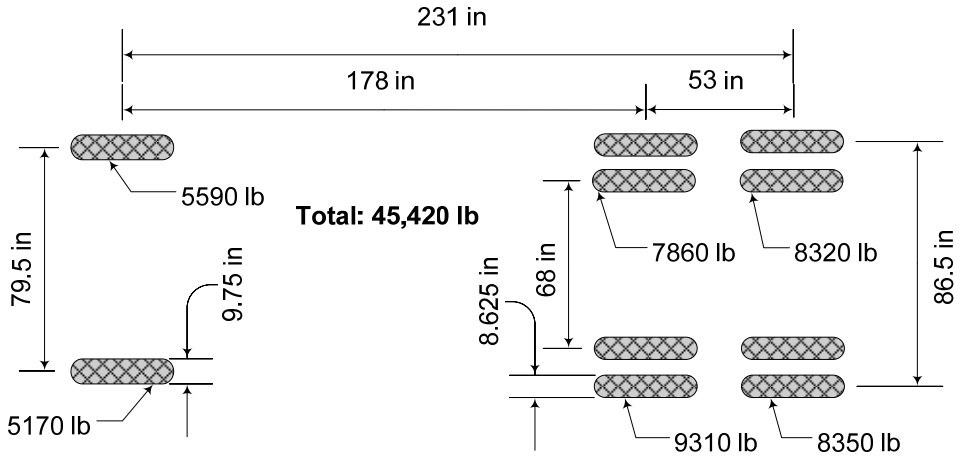

Figure 41: Axle dimensions and associated weights of test vehicle.

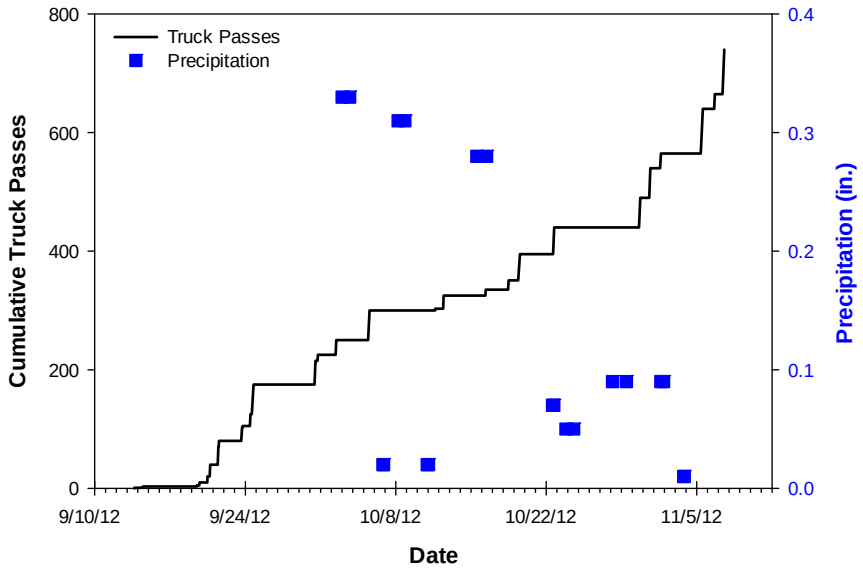

Figure 42: Precipitation events that occurred during trafficking.

Figure 43: Rut repair: a) adding gravel to the rutted area, b) compacting the new gravel with the skid-steer tractor, and c) final smoothing.

Rut measurements were made at 40-inch intervals along two longitudinal lines that corresponded to the outside rear wheels of the test vehicle using a robotic total station. Twenty-eight longitudinal rut measurements were made in each test section at various trafficking levels (14 in the east rut and 14 in the west rut). A summary of the measurements timetable is shown in Table 7. Transverse rut measurements were also made at these same times in two locations in each test section (geographically coincident with the instrumentation locations). Sixteen individual measurements were taken to create a single transverse surface contour.

Table 7: Summary of Rut Measurements

Date Measured	Truck Passes	Notes
9/13/2012	0	
9/14/2012	3	
9/19/2012	10	
9/20/2012	20	
9/20/2012	40	
9/21/2012	70	C1 only
9/23/2012	80	
9/23/2012	102	C1 only
9/24/2012	125	2, 7 and 9 only
9/25/2012	175	
10/2/2012	250	
10/9/2012	300	
10/15/2012	325	
10/18/2012	351	
10/19/2012	395	
10/29/2012	440	
11/1/2012	540	
11/6/2012	640	
11/19/2012	740	

These measurements will be used to determine rut as a function of the difference in the elevation of the measurement points over time. Total rut, therefore, will be determined by comparing current measurements to a baseline measurement which was made before trafficking. This type of rut is referred to as "elevation rut", as illustrated in Figure 44. The "apparent rut", however, is typically greater and can be defined as the vertical distance from the upper crest of the rut bowl to the bottom of the rut bowl (Figure 44). The rutting results have not been fully analyzed yet and are, therefore, not ready to be presented.

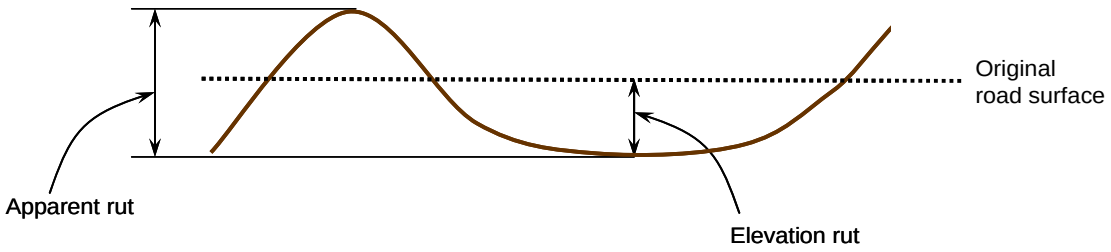

Figure 44. Illustration of rut measurements.

References

Cuelho, E.; Perkins, S.; Hauck, J. and Akin, M. (2009) "Field Investigation of Geosynthetics Used for Subgrade Stabilization," Final report to the Montana Department of Transportation, FHWA/MT-09-003/8193.

Holtz, R.D., Christopher, B.R., Berg, R.R. (2008) Geosynthetic Design and Construction Guidelines, FHWA-NHI-07-092, Federal Highway Administration Washington, D.C., 592 p.

Kessler Soils Engineering Products, Inc. (2010) KSE DCP K-100 Models with Quick Connect Pin User's Manual, 36p.

Peck, R.B., Hansen, W.E., and Thornburn, T.H. (1974) *Foundation Engineering*, 2nd ed., Wiley, New York.

Appendix A–History of Rut Repair for All Test Sections

The following tables provide a visual history of the rut repair for all of the test sections during trafficking. Twenty-eight rut measurements were made in each test section (14 in the east rut and 14 in the west rut). Each of these measurements is represented by a single box in the following tables. Boxes that are shaded indicate when ruts were filled and measurements in those areas were ended.

Test Section IFG-1																
Truck Pass	Rut	Measurement Point														
		1	2	3	4	5	6	7	8	9	10	11	12	13	14	
0	E															
	W															
3	E															
	W															
10	E															
	W															
20	E															
	W															
40	E															
	W															
70	E															
	W															
80	E															
	W															
102	E															
	W															
125	E															
	W															
175	E															
	W															
250	E															
	W															
300	E															
	W															
325	E															
	W															
351	E															
	W															
395	E															
	W															
440	E															
	W															
540	E															
	W															
640	E															
	W															
740	E															
	W															

Test Section IFG-2																
Truck Pass	Rut	Measurement Point														
		1	2	3	4	5	6	7	8	9	10	11	12	13	14	
0	E															
	W															
3	E															
	W															
10	E															
	W															
20	E															
	W															
40	E															
	W															
70	E															
	W															
80	E															
	W															
102	E															
	W															
125	E															
	W															
175	E															
	W															
250	E															
	W															
300	E	■	■	■	■	■	■	■				■	■	■		
	W	■	■	■	■	■	■	■				■	■	■	■	
325	E	■	■	■	■	■	■	■				■	■	■		
	W	■	■	■	■	■	■	■				■	■	■	■	
351	E	■	■	■	■	■	■	■				■	■	■		
	W	■	■	■	■	■	■	■				■	■	■	■	
395	E	■	■	■	■	■	■	■				■	■	■		
	W	■	■	■	■	■	■	■				■	■	■	■	
440	E	■	■	■	■	■	■	■				■	■	■		
	W	■	■	■	■	■	■	■				■	■	■	■	
540	E	■	■	■	■	■	■	■				■	■	■		
	W	■	■	■	■	■	■	■				■	■	■	■	
640	E	■	■	■	■	■	■	■	■	■	■	■	■	■		
	W	■	■	■	■	■	■	■	■	■	■	■	■	■	■	
740	E	■	■	■	■	■	■	■	■	■	■	■	■	■		
	W	■	■	■	■	■	■	■	■	■	■	■	■	■	■	

Test Section IFG-3															
Truck Pass	Rut	Measurement Point													
		1	2	3	4	5	6	7	8	9	10	11	12	13	14
0	E														
	W														
3	E														
	W														
10	E														
	W														
20	E														
	W														
40	E														
	W														
70	E														
	W														
80	E														
	W														
102	E														
	W														
125	E														
	W														
175	E														
	W														
250	E														
	W														
300	E														
	W														
325	E														
	W														
351	E														
	W														
395	E														
	W														
440	E														
	W														
540	E														
	W														
640	E														
	W														
740	E														
	W														

Test Section WeG-4															
Truck Pass	Rut	Measurement Point													
		1	2	3	4	5	6	7	8	9	10	11	12	13	14
0	E														
	W														
3	E														
	W														
10	E														
	W														
20	E														
	W														
40	E														
	W														
70	E														
	W														
80	E														
	W														
102	E														
	W														
125	E														
	W														
175	E														
	W														
250	E														
	W														
300	E														
	W														
325	E														
	W														
351	E														
	W														
395	E														
	W														
440	E														
	W														
540	E														
	W														
640	E														
	W														
740	E														
	W														

Test Section WeG-5															
Truck Pass	Rut	Measurement Point													
		1	2	3	4	5	6	7	8	9	10	11	12	13	14
0	E														
	W														
3	E														
	W														
10	E														
	W														
20	E														
	W														
40	E														
	W														
70	E														
	W														
80	E														
	W														
102	E														
	W														
125	E														
	W														
175	E														
	W														
250	E														
	W														
300	E														
	W														
325	E														
	W														
351	E														
	W														
395	E														
	W														
440	E														
	W														
540	E														
	W														
640	E														
	W														
740	E														
	W														

Test Section WoG-6															
Truck Pass	Rut	Measurement Point													
		1	2	3	4	5	6	7	8	9	10	11	12	13	14
0	E														
	W														
3	E														
	W														
10	E														
	W														
20	E														
	W														
40	E														
	W														
70	E														
	W														
80	E														
	W														
102	E														
	W														
125	E														
	W														
175	E														
	W														
250	E														
	W														
300	E														
	W														
325	E														
	W														
351	E														
	W														
395	E														
	W														
440	E														
	W														
540	E														
	W														
640	E														
	W														
740	E														
	W														

Test Section WoG-7															
Truck Pass	Rut	Measurement Point													
		1	2	3	4	5	6	7	8	9	10	11	12	13	14
0	E														
	W														
3	E														
	W														
10	E														
	W														
20	E														
	W														
40	E														
	W														
70	E														
	W														
80	E														
	W														
102	E														
	W														
125	E														
	W														
175	E														
	W														
250	E														
	W														
300	E														
	W														
325	E														
	W														
351	E														
	W														
395	E														
	W														
440	E														
	W														
540	E														
	W														
640	E														
	W														
740	E														
	W														

Test Section WoG-8															
Truck Pass	Rut	Measurement Point													
		1	2	3	4	5	6	7	8	9	10	11	12	13	14
0	E														
	W														
3	E														
	W														
10	E														
	W														
20	E														
	W														
40	E														
	W														
70	E														
	W														
80	E														
	W														
102	E														
	W														
125	E														
	W														
175	E														
	W														
250	E														
	W														
300	E														
	W														
325	E														
	W														
351	E														
	W														
395	E														
	W														
440	E														
	W														
540	E														
	W														
640	E														
	W														
740	E														
	W														

Test Section KnG-9															
Truck Pass	Rut	Measurement Point													
		1	2	3	4	5	6	7	8	9	10	11	12	13	14
0	E														
	W														
3	E														
	W														
10	E														
	W														
20	E														
	W														
40	E														
	W														
70	E														
	W														
80	E														
	W														
102	E														
	W														
125	E														
	W														
175	E														
	W														
250	E														
	W														
300	E														
	W														
325	E														
	W														
351	E														
	W														
395	E														
	W														
440	E														
	W														
540	E														
	W														
640	E														
	W														
740	E														
	W														

Test Section ExG-10															
Truck Pass	Rut	Measurement Point													
		1	2	3	4	5	6	7	8	9	10	11	12	13	14
0	E														
	W														
3	E														
	W														
10	E														
	W														
20	E														
	W														
40	E														
	W														
70	E														
	W														
80	E														
	W														
102	E														
	W														
125	E														
	W														
175	E														
	W														
250	E														
	W														
300	E														
	W														
325	E														
	W														
351	E														
	W														
395	E														
	W														
440	E														
	W														
540	E														
	W														
640	E														
	W														
740	E														
	W														

Test Section IFG-11															
Truck Pass	Rut	Measurement Point													
		1	2	3	4	5	6	7	8	9	10	11	12	13	14
0	E														
	W														
3	E														
	W														
10	E														
	W														
20	E														
	W														
40	E														
	W														
70	E														
	W														
80	E														
	W														
102	E														
	W														
125	E														
	W														
175	E														
	W														
250	E														
	W														
300	E														
	W														
325	E														
	W														
351	E														
	W														
395	E														
	W														
440	E														
	W														
540	E														
	W														
640	E														
	W														
740	E														
	W														

Test Section IFG-12															
Truck Pass	Rut	Measurement Point													
		1	2	3	4	5	6	7	8	9	10	11	12	13	14
0	E														
	W														
3	E														
	W														
10	E														
	W														
20	E														
	W														
40	E														
	W														
70	E														
	W														
80	E														
	W														
102	E														
	W														
125	E														
	W														
175	E														
	W														
250	E														
	W														
300	E														
	W														
325	E														
	W														
351	E														
	W														
395	E														
	W														
440	E														
	W														
540	E														
	W														
640	E														
	W														
740	E														
	W														

Test Section WoT-13															
Truck Pass	Rut	Measurement Point													
		1	2	3	4	5	6	7	8	9	10	11	12	13	14
0	E														
	W														
3	E														
	W														
10	E														
	W														
20	E														
	W														
40	E														
	W														
70	E														
	W														
80	E														
	W														
102	E														
	W														
125	E														
	W														
175	E														
	W														
250	E														
	W														
300	E														
	W														
325	E														
	W														
351	E														
	W														
395	E														
	W														
440	E														
	W														
540	E														
	W														
640	E														
	W														
740	E														
	W														

Test Section NWoT-14															
Truck Pass	Rut	Measurement Point													
		1	2	3	4	5	6	7	8	9	10	11	12	13	14
0	E														
	W														
3	E														
	W														
10	E														
	W														
20	E														
	W														
40	E														
	W														
70	E														
	W														
80	E														
	W														
102	E														
	W														
125	E														
	W														
175	E														
	W														
250	E														
	W														
300	E														
	W														
325	E														
	W														
351	E														
	W														
395	E														
	W														
440	E														
	W														
540	E														
	W														
640	E														
	W														
740	E														
	W														

Test Section Control 1															
Truck Pass	Rut	Measurement Point													
		1	2	3	4	5	6	7	8	9	10	11	12	13	14
0	E														
	W														
3	E														
	W														
10	E														
	W														
20	E														
	W														
40	E														
	W														
70	E														
	W														
80	E														
	W														
102	E														
	W														
125	E														
	W														
175	E														
	W														
250	E														
	W														
300	E														
	W														
325	E														
	W														
351	E														
	W														
395	E														
	W														
440	E														
	W														
540	E														
	W														
640	E														
	W														
740	E														
	W														

Test Section Control 2															
Truck Pass	Rut	Measurement Point													
		1	2	3	4	5	6	7	8	9	10	11	12	13	14
0	E														
	W														
3	E														
	W														
10	E														
	W														
20	E														
	W														
40	E														
	W														
70	E														
	W														
80	E														
	W														
102	E														
	W														
125	E														
	W														
175	E														
	W														
250	E														
	W														
300	E														
	W														
325	E														
	W														
351	E														
	W														
395	E														
	W														
440	E														
	W														
540	E														
	W														
640	E														
	W														
740	E														
	W														

Test Section Control 3															
Truck Pass	Rut	Measurement Point													
		1	2	3	4	5	6	7	8	9	10	11	12	13	14
0	E														
	W														
3	E														
	W														
10	E														
	W														
20	E														
	W														
40	E														
	W														
70	E														
	W														
80	E														
	W														
102	E														
	W														
125	E														
	W														
175	E														
	W														
250	E														
	W														
300	E														
	W														
325	E														
	W														
351	E														
	W														
395	E														
	W														
440	E														
	W														
540	E														
	W														
640	E														
	W														
740	E														
	W														